ACS APPLIED ENERGY MATERIALS

www.acsaem.org

Review

Deep Eutectic Solvents: Physicochemical Properties and Challenges in Applications as Phase Change Materials in Thermal Energy Storage

Published as part of ACS Applied Energy Materials special issue "Energy Storage across Scales".

Nouman Rafique, Mihkel Koel, Dinis O. Abranches, and Oliver Järvik*

Cite This: https://doi.org/10.1021/acsaem.5c02743

Read Online

ACCESS | Metrics & More | Article Recommendations | Supporting Information

ABSTRACT: Deep eutectic solvents (DESs) have emerged as versatile and highly tunable solvents for a variety of applications. This review explores properties of different DES-based phase change materials (PCMs), highlighting their potential and challenges for latent heat thermal energy storage (LHTES). Key challenges such as supercooling, thermal stability, thermal conductivity, and thermophysical properties such as melting temperature, heat of fusion, heat capacities, viscosities, and densities of DESs are discussed along with strategies to improve their thermophysical properties. By reviewing recent advances, this study aims to provide a comprehensive understanding of DESs as next-generation PCMs for renewable energy applications. This work is also a source of curated, extensive data sets for future research directions in the field of LHTES systems and related applications.

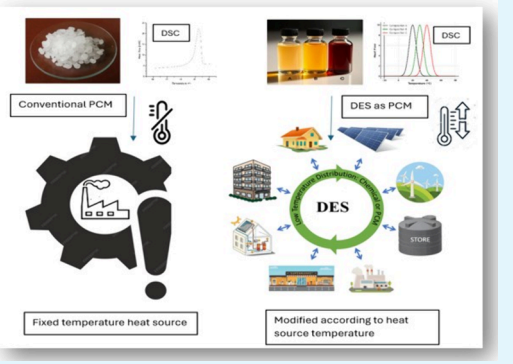

KEYWORDS: *thermal energy storage, thermophysical properties, phase change materials, deep eutectic solvents, heat transfer fluids, thermal conductivity, nanomaterials additives, waste heat recovery*

1. INTRODUCTION

It is worth noting that deep eutectic solvents (DESs) have been defined in a variety of ways to emphasize their physicochemical properties. In this review the definition by Martins et al.[1] is adopted stating that DES is a mixture of two or more pure compounds for which the eutectic point temperature is below that of an ideal liquid mixture, exhibiting significant negative deviations from ideality ($\Delta T_2 > 0$), where ΔT_2 represents the temperature depression, i.e., the difference between the ideal and the real eutectic points. This definition provides a quantitative and generalizable criterion based on measurable thermodynamic behavior. The deviation of T_m from ideality is due to the formation of hydrogen bonds, thus coining the terms Lewis or Brønsted acid or hydrogen bond donor (HBD) and Lewis or Brønsted base or hydrogen bond acceptor (HBA) for the components of DESs.[2,3] Although sometimes grouped together, DESs are different from ionic liquids (ILs). While both classes of solvents offer tunable properties for different applications, ILs are pure salts with low melting points (usually comprised of an organic cation and an organic or inorganic anion), whereas DESs are mixtures formed by combining two pure compounds, one acting as an HBD and the other as an HBA. They differ in composition (pure salt vs mixture), type of interactions (ionic vs hydrogen bonding), and method of formation (synthesis vs physical mixing). The wide range of starting materials allows customization, making both ILs and DESs valuable in many scientific and technological fields.[4,5]

DESs are considered to be greener and cheaper alternatives to traditional solvents, in part because most researchers for DES preparation prefer precursors that are usually naturally occurring. For example, precursors such as choline chloride (ChCl), urea (U), glycerol (Gly), lactic acid (2-HPA), carboxylic acids, polyalcohol, amino acids, and vitamins are typically derived from renewable sources. DES formulated from naturally occurring precursors are termed natural deep eutectic solvents (NADESs). For simplicity of the manuscript, NADESs are also covered under the broader term "DES." As a result, DESs often exhibit high biodegradability and low toxicity.[6,7] However, generalizing these traits to all DESs is problematic, due to the simple formation strategy and diverse precursors, just as they have been overused in studies of ILs.[1,3,8] In fact, this generalization has been criticized in the

Received: September 1, 2025
Revised: December 9, 2025
Accepted: December 12, 2025

Table 1. Common Types of PCM Categories, along with Temperature Ranges and Examples

category	subcategory	temperature range, °C	examples
inorganic salts		medium to very high (150 to 1500)	$NaNO_3$, $LiNO_3$, $MgCl_2$, KOH, LiH, KF
organic		low to medium (20 to 200)	LA, SA, erythritol, *n*-pentadecane, *n*-hexadecane, *n*-heptadecane, *n*-henicosane, *n*-tricosane
eutectics	molten salts	high (200 to 1000)	LiF:NaF:CaF_2, NaOH:NaCl:Na_2CO_3, NaF:$NaNO_3$:NaCl, NaF:NaBr, NaF:NaCl, NaF:CaF_2:MgF_2, NaCl:$MgCl_2$
	DESs	very low to medium (−20 to 200)	LA:PA:SA, LA:SA, LA:PA, LA:MA, LA:1,6-hexanediol, LA:SA, LA: methyl palmitate, LA: myristic alcohol
salt hydrates		low to medium (30 to 150)	$CaCl_2{\cdot}6H_2O$, $MgCl_2{\cdot}6H_2O$, $Na_2P_2O_7{\cdot}10H_2O$, $Ba(OH)_2{\cdot}8H_2O$, $FeCl_3{\cdot}6H_2O$, $KF{\cdot}4H_2O$
composites		low to medium (20 to 200)	(26.6 wt %) wallboard, paraffin (75 wt %) silica ceramic, capric−stearic acid (25 wt %) gypsum, RT20/montmorillonite, beeswax/graphene, PW/rGO/MOF, gold tailing/solar salt, SA/BA/graphite, CFA (coal fly ash)/K_2CO_3, SiO_2/Na_2SO_4, Al_2O_3/Na_2SO_4, Si_3N_4/NaCl-KCl-$MgCl_2$

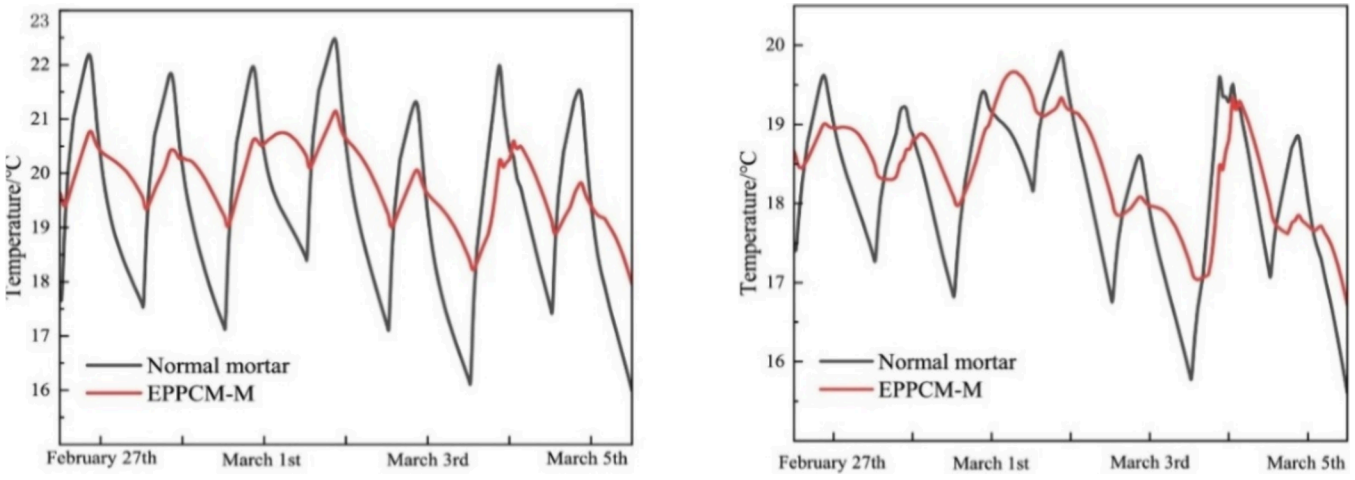

Figure 1. Seven day temperature variation curves of the floor surfaces (left) and indoor air temperature (right) (reported uncertainty = ± 0.3 °C). Reprinted with permission from ref 21. Copyright 2025 Elsevier

past,[9] as many nonsustainable precursors can also yield DESs. Thus, their "green" character should be assessed individually. While DESs differ conceptually from ILs, they share similar physicochemical properties like low to negligible vapor pressure, high thermal stability, nonflammability, high conductivity, and ease of recycling,[10] though these vary depending on the precursors used.[11] Recently, many have been found to be, in fact, volatile, flammable, and even toxic.[5]

Although many DESs are hydrophilic due to the presence of salts, they can also be hydrophobic. For example, van Osch et al.[12] introduced hydrophobic DESs (HDES) as water-immiscible extractants. Ribeiro et al.[13] prepared low-viscosity HDES from two neutral components (menthol and several organic acids). The hydrophobic or hydrophilic nature of DES can be attributed to the nature of the starting materials on the basis of reported data. Long alkyl chains and a lack of ionicity in the HBD usually result in HDES.[12] Ribeiro et al.[13] classified many type III and type V DESs as HDESs.

2. PHASE CHANGE MATERIALS IN THERMAL ENERGY STORAGE

Thermal energy storage (TES) is a key technology that enables the effective integration of renewable energy sources into future smart energy systems and advanced energy networks. In the case where the thermal energy demand is met by a fluctuating heat source such as solar or industrial waste heat, TES can be used to provide constant or more predictable heat production. Traditionally, in large-scale thermal energy storage installations, sensible heat storage systems are the most commonly employed due to their simplicity, low cost, and well-established operational reliability,[14] although TES systems can be based on sensible heat, latent heat, and thermochemical heat. Water, steam, sand, and concrete are the main materials used to store sensible heat. Sensible TES systems, working by just a temperature change, can achieve a low cost and can be appropriate in some cases, but they also have a low energy density and take a lot of space, meaning a large mass of material is needed to store a significant amount of energy. By contrast, to increase the energy density of a TES system, latent heat thermal energy storage (LHTES) systems based on the heat of fusion ($\Delta_{fus}h$) of a phase change material (PCM), are preferred. In general, the thermal energy stored in a material is the sum of its latent and sensible energy according to eq 1.

$$Q = \int_{T_i}^{T_m} mC_{p,s}\mathrm{d}T + xm\Delta_{fus}h + \int_{T_m}^{T_f} mC_{p,l}\mathrm{d}T \quad (1)$$

where T_i is the initial temperature, °C or K, T_m is the melting temperature, °C or K, T_f is the final temperature, °C or K, $C_{p,l}$ and $C_{p,s}$ are specific heat capacities of liquid and solid phases, J $kg^{-1}K^{-1}$, respectively, m is the mass of PCM, kg, x is the fraction of melted PCM, $\Delta_{fus}h$ is the heat of fusion, J kg^{-1}.

2.1. Comparison of PCMs. Many PCMs are being used in TES applications, broadly categorized as inorganic salt hydrates and molten salts, organic compounds, including fatty acids and paraffin waxes, and eutectic materials. Common organic, inorganic, and eutectic PCMs are listed in Table 1.

https://doi.org/10.1021/acsaem.5c02743
ACS Appl. Energy Mater. XXXX, XXX, XXX−XXX

Molten salts have long been used in energy applications due to their high specific heat capacities.[15−20] However, molten salts are limited by their high T_m, typically above 200 °C, which poses maintenance challenges at lower temperatures.[19] Using LHTES with a T_m closer to the application temperature can reduce heat loss during the operation. DES, which offers significant tuning potential, could be a suitable alternative to molten salt PCMs.

Salt hydrates are low-toxic, abundant, and cost-effective, but can cause corrosion and potential environmental contamination. Paraffins, derived from petroleum, are stable and durable but raise concerns due to their fossil origin, flammability, and persistence in the environment. DESs, made from biodegradable, low-toxicity components, offer green chemistry benefits such as low volatility and recyclability; however, further study is required to confirm their long-term sustainability. Overall, DESs present fewer environmental hazards throughout their lifecycle than paraffins, while salt hydrates remain cost-effective with proper disposal management.

2.2. Comparative Performance of PCMs from a Case Study of Indoor Air Temperature Fluctuations. Recent advances in building-integrated TES have introduced salt hydrates and eutectic PCMs to enhance indoor temperature regulation. Liu et al.[21] developed an epicyclic PCM, a hydrated salt-based composite for radiant floor heating, which reduces temperature fluctuations by 55% on floors and 40% in indoor air, while maintaining stable $\Delta_{fus}h$ across cycles and limiting daily temperature variation to 2.5 °C (Figure 1). However, challenges such as phase segregation and dehydration remain, requiring stabilization and encapsulation strategies.

In contrast, Brahimi et al.[22] investigated eutectic PCM mixtures embedded in hollow clay bricks. They found that the heat fluctuation at the inner surface decreased by approximately 58% compared to that of a conventional hollow clay wall, with temperature fluctuations remaining within 2.8 °C (Figure 2).

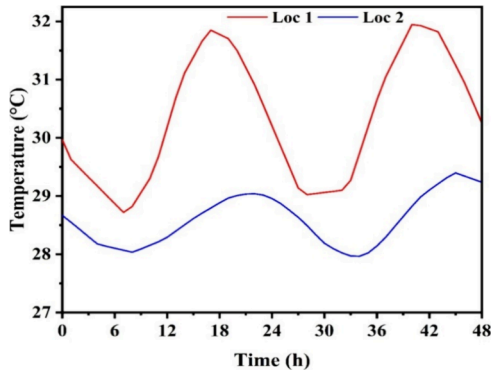

Figure 2. Internal surface temperature variations for the wall with (Loc 2) and without PCM (Loc 1) (reported uncertainty = ± 1 °C). Reprinted with permission from ref 22. Copyright 2025 Elsevier.

Vighnesh et al.[23] proposed a shape-stabilized PCM/vermiculite (EV-PCM) composite integrated into concrete roofing elements. They optimized parameters such as PCM loading, geometry, and composite structure to reduce indoor temperature fluctuations and spikes in the roof surface temperature. The tested EV-PCM composite lowered indoor air temperature fluctuation values by 3.75−9.48%, performing better than conventional roofs (20.73−21.42%) (Figure 3).

The $\Delta_{fus}h$ values for the salt hydrate, eutectic, and composite PCMs are reported as 156, 200, and 58 J g^{-1}, respectively.[21−23] These results emphasize the feasibility of using eutectic PCMs for passive TES. Although composite PCMs have superior integration compatibility compared with salt hydrates and eutectics, they have a very low energy storage capacity.

2.3. Comparative Economic Analysis. In terms of technological readiness and availability, paraffins are the most developed PCMs, followed by salt hydrates, fatty acids, and composites. Many salt hydrates have low material costs (≈$0.1−$5/kg), a high $\Delta_{fus}h$ (100−290 J g^{-1}), and a high density (1.3−2.6 g cm^{-3}).[24] This results in favorable volumetric storage density and low energy storage costs (≈50−130 kWh m^{-3} and $ 0.90−$4.00/kWh, respectively).[24] However, some salts are notably more expensive due to scarcity or competition from other industries, such as lithium-based salts. The corrosive salt hydrates require safety measures, which aid their long-term operational cost.

Paraffins have the lowest energy storage cost in the temperature range of 8−17 °C at 6.50−40 $/kWh.[24] Despite having favorable $\Delta_{fus}h$ (150−250 J g^{-1}), their low density (0.8−0.95 g cm^{-3}) results in poor volumetric storage capacity (32−80 kWh m^{-3}).[25−27] Fatty acids generally have high material costs ($ 2.50−200/kg), leading to high energy storage costs ($40−3,000/kWh).[28] Their $\Delta_{fus}h$ and density are similar to those of fatty acids.[28] Low-molecular-weight paraffins are usually volatile and flammable, which adds to their safety and handling costs.

Salt hydrates are easy to prepare and often do not require complex synthesis. They can be used as they are or mixed with water or combined with impurities, depending on the application. Paraffins used as PCMs may need purification and encapsulation, but sometimes they are used in raw or technical grade form. DESs are produced in a single step through low-energy mixing without the use of solvents, which reduces both capital and operational costs. They are nonvolatile and nonflammable, so safety and handling costs are also reduced during large-scale manufacturing and storage.

Apparently, the cost of DESs can range between salt hydrates and paraffin PCMs, depending on the preparation method, precursors, and integration of materials into the technology.

2.4. Integration into Technology. Salt hydrates and paraffins are well-established, cost-effective PCMs, used in cold storage, and sold by companies like Rubitherm GmbH, Climator, and PCM Products. Stabilized salt hydrates are also applied in TES systems, including heating, ventilation, and cooling systems (HVAC), and cold chain logistics by companies like PLUSS and Phase Change Energy Solutions.

In contrast, DESs are still in development but show potential for industrial applications. A pilot-scale study demonstrated their use in solar drying after sunset; 5 kg of stearyl alcohol and benzamide and 3 kg of PA-SA (palmitic acid−stearic acid) were evaluated separately. The thermal performance of solar dryers extended up to 4 and 4.5 h, compared to the systems without DESs.[29,30] On an industrial scale, DESs can be integrated into thermal batteries, as illustrated in Figure 4.

In the basic absorption thermal battery, NH_3/Glyceline, a working DES fluid, achieves competitive energy storage efficiency and exergy efficiency compared to the commonly used H_2O/LiBr and even outperforms H_2O/LiBr under inferior operating conditions (generation temperature <72 °C, evaporating temperature <1 °C, or absorption temperature >40 °C).[32] With DESs, the compression-assisted thermal battery provides higher energy storage efficiency, energy storage density, and exergy efficiency concentration glide than the basic absorption thermal battery.[32]

DESs have also shown potential for direct use in solar power plants. For example, Peyrovedin et al.[33] investigated seven different DESs in systems coupled with organic Rankine cycles to assess their power generation performance. Their analysis revealed that certain DESs outperform paraffins in both energy and exergy efficiency. Notably, the cycle utilizing DES ChCl:4-HBA generated 25% more power compared to the cycle using paraffin as the PCM.

In a study by Sui et al.[34] DESs were used as both the absorbent and active TES medium in a multicell absorption thermal energy storage (MATES) system (Figure 5). This approach effectively addressed key limitations of conventional PCM-based systems, such as crystallization and heat loss. By utilizing DESs with tailored phase behavior and high energy storage densities, reaching up to 550 J g^{-1}, the system achieved stable discharge performance and efficiently harnessed low-grade solar heat (<50 °C). Aligning the T_m of DES with the operating range minimized thermal gradients and heat losses, resulting in economic viability with storage costs of 0.032−0.040 USD/kWh.

https://doi.org/10.1021/acsaem.5c02743
ACS Appl. Energy Mater. XXXX, XXX, XXX−XXX

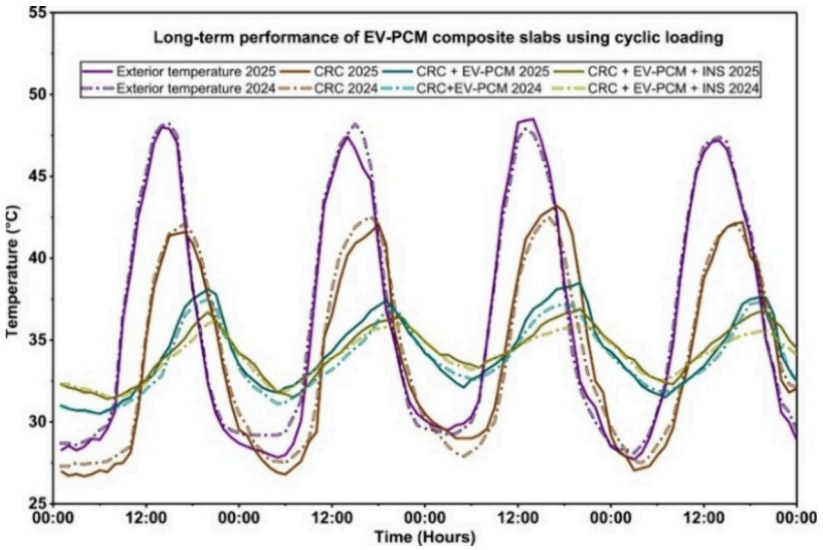

Figure 3. Thermal performance of EV-PCM composite slab configurations for March 2024 and 2025. EV-PCM (reported uncertainty = ±2 °C). (CRC + EV-PCM + INS represents a conventional roof integrated with EV-PCM and insulation). Reprinted with permission from ref 23. Copyright 2025 Elsevier.

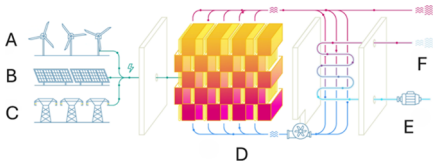

Figure 4. Concept of the Rondo thermal battery. Electricity from different sources—wind (A), solar (B), and grid (C) is converted into heat and stored in PCM (D). The stored heat is then used to convert cold water (E) into steam (F). Reprinted with permission from ref 31.

These findings highlight DESs as promising, cost-effective, and scalable PCMs for seasonal and low-temperature TES applications.

A similar idea could be extended to the use of DESs as thermal comfort agents in buildings, utilizing a two-container principle for heat exchange, as illustrated in Figure 6.[35] The PCM-based system operates in two modes: direct cooling during the day, where the melting PCM absorbs excess heat from indoor air and recirculates the cooled air back into the room; and nighttime heat release, where the stored heat in the PCM warms incoming outdoor air when external temperatures fall below indoor levels. The system's efficiency depends on the alignment between the daytime temperature range (between 12 and 15 °C)[36] and the T_m of the PCM (ideally between 19 and 24 °C).[37]

2.5. Challenges of PCMs. One major issue sometimes encountered with PCMs, and potentially with DES-based systems, is metastability, particularly supercooling. This phenomenon occurs when a liquid cools below its freezing point without solidifying,[38−40] due to the failure of molecules to organize into a crystal lattice upon reaching the temperature barrier (Figure 7).

In salt hydrates, supercooling arises because water molecules remain trapped in hydration shells around the cations, creating a metastable liquid state even at temperatures well below the thermodynamic freezing point (eq 2).

$$\text{Salt}\cdot x\text{H}_2\text{O(l)} \xrightarrow{\text{supercooling}} \text{Salt} + x\text{H}_2\text{O(l)} \quad (2)$$

Similarly, DESs may experience supercooling due to ionic disorder, which stabilizes the liquid phase and prevents molecular ordering. Forming a eutectic crystal requires precise stoichiometric alignment

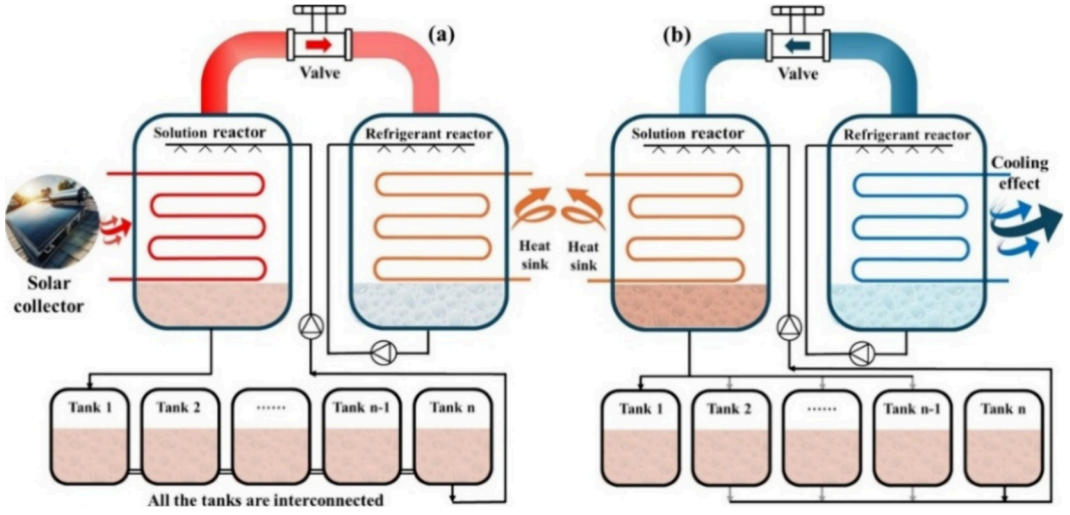

Figure 5. Schematic diagrams of the MATES cycle: (a) charging process and (b) discharging process. Reprinted with permission from ref 34. Copyright 2025 Elsevier.

https://doi.org/10.1021/acsaem.5c02743
ACS Appl. Energy Mater. XXXX, XXX, XXX−XXX

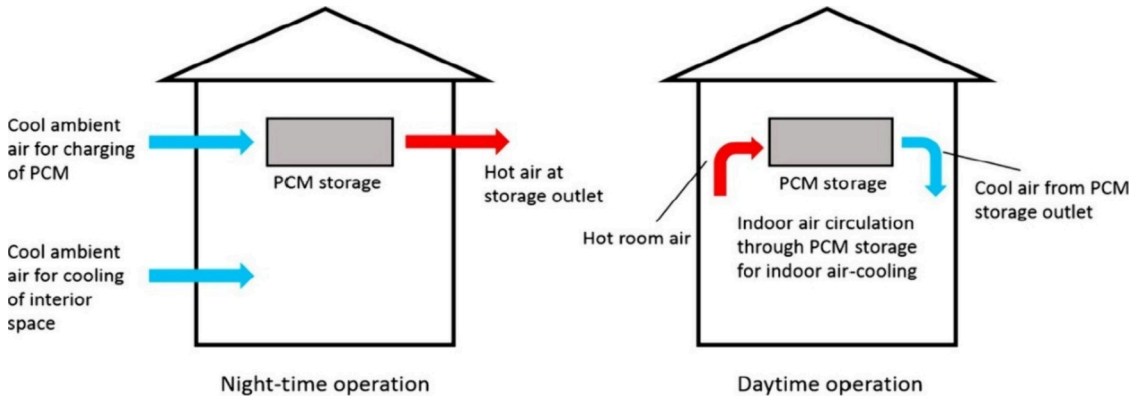

Figure 6. Two operation modes of the free cooling system. Reprinted with permission from ref 35. Copyright 2019 Elsevier.

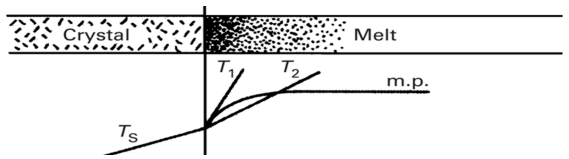

Figure 7. Ordering of molecules upon reaching freezing point. Reprinted with permission from ref 41. Copyright 2001 Elsevier.

and hydrogen bond rearrangement between components; any compositional deviation can delay nucleation. In contrast, paraffin-based PCMs exhibit minimal supercooling due to their regular van der Waals interactions and high molecular symmetry, which promote lattice formation upon cooling.[42]

Minimizing supercooling is critical for improving the efficiency and reliability of LHTES systems.[43] Incomplete freezing of PCMs can hinder heat release, especially when the heat transfer fluid (HTF) temperature approaches the T_m of the PCM, complicating system control.[44]

Some paraffins, such as dodecane and tetradecane, exhibit minimal supercooling.[44] On the other hand, paraffins, while chemically stable, have low thermal conductivity, limiting heat transfer rates during charging and discharging. They are also combustible, posing safety risks, particularly on large scales or open systems. Volume changes during melting and solidification can lead to a system leakage or structural stress unless properly managed.[45] Moreover, paraffins are nonbiodegradable, raising environmental concerns.

Salt hydrates have additionally material-specific challenges like corrosivity to metal containers and system components.[46] During solid–liquid phase transitions, salt hydrates may leak if not properly contained, particularly when the water of crystallization separates. This necessitates the use of special materials for encapsulation and system design, which can increase costs and complexity.[46]

All PCMs face similar implementation and reliability issues. For DESs, the primary concern is the lack of consistent and reliable thermophysical data, particularly for heat capacity (C_p), $\Delta_{fus}h$, thermal conductivity (λ), and T_m. Standardized testing and rigorous experimental validation are essential to improving data reliability and comparability.

While some research has focused on heat and mass transfer processes in PCMs[47−49] for TES applications, a gap remains in translating these findings into the design and optimization of practical thermal energy devices.

From a design perspective, a DES intended for use as a PCM should possess a combination of thermophysical properties that support efficient and reliable TES. High $\Delta_{fus}h$ and C_p, per unit volume and per mass, are crucial for maximizing storage potential. The T_m must align with the operational range of the intended application to ensure effective energy absorption and release. Additionally, maintaining a low vapor pressure at operating temperatures is critical to prevent leakage and ensure long-term material stability. For consistent performance, the material should crystallize reproducibly without degradation over repeated thermal cycles. Minimizing supercooling and enabling rapid crystal growth enhances thermal responsiveness and energy efficiency. Furthermore, high thermal conductivity is needed for facilitating effective heat transfer during both the charging and discharging phases, ultimately improving the overall performance of the TES system.

3. CHARACTERISTICS OF REQUIRED DESS TO FUNCTION AS PCM

Relevant properties of DESs to be used in LHTES are discussed in the following sections.

3.1. Melting Point of DESs. The T_m is crucial in designing PCM materials. For HVAC, a T_m of around 15−25 °C is ideal, while medium temperature storage (80−150 °C) suits solar thermal and waste heat recovery. High-temperature PCMs are needed for industrial heat storage and thermal batteries.[50] To maximize performance, the PCM should undergo a phase change as close as possible to the target operating temperature. Selection criteria for T_m vary depending on the application, and careful matching ensures efficient energy storage and release.

The desired T_m for a specific application can be achieved by studying factors such as component variation, mole ratio adjustments of binary DES mixtures, and additives. The primary focus is on understanding how these factors affect the T_m of DESs, as described by the Schroeder−Van Laar equation.[51]

The Schroeder−Van Laar equation[51] is a foundational tool in physical chemistry and thermodynamics used to predict the phase behavior of mixtures. This "ideal" prediction is a baseline, assuming the components mix perfectly without any special attractive or repulsive forces between them and assuming a constant $\Delta_{fus}h$ (eq 3).

$$\ln(x_i\gamma_i) = \frac{\Delta_{fus}h_i}{R}\left(\frac{1}{T_{m,i}} - \frac{1}{T_m}\right) \quad (3)$$

where, x_i is the mole fraction of component i, γ_i is the activity coefficient (for an ideal mixture, $\gamma_i = 1$), $\Delta_{fus}h$ is the enthalpy of fusion of component i, $T_{m,i}$ is the melting point of the pure component, T_m is the melting temperature of the mixture, and R is the general gas constant.

Application of this equation gives a solid–liquid phase diagram representing the T_m of DES (Figure 8).

The observed low T_m for a DES is achieved because the intermolecular interaction between the HBA and HBD in the liquid mixture is stronger than the crystal lattice energy in the

https://doi.org/10.1021/acsaem.5c02743
ACS Appl. Energy Mater. XXXX, XXX, XXX−XXX

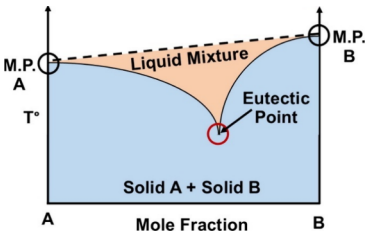

Figure 8. Phase diagram for the binary mixture DES.[52] Note that the dashed line represents composition-average T_m but holds no physical meaning. Reprinted with permission from ref 52. Copyright 2022 Elsevier.

pure solid components.[53] The specific ratio and complementary nature of the components maximize the structural disorder i.e., $\Delta_{fus}S$ is higher than ideal in the liquid phase, further depressing the T_m (eq 4[54]).

$$T_m = \frac{\Delta_{fus}h}{\Delta_{fus}S} \tag{4}$$

The eq 3 shows the trend of the T_m change of a binary mixture and can be used to estimate the approximate composition of the eutectic mixture (mixture with the lowest T_m); however, calculated T_m results can be quite different from the actual values when deviations from thermodynamic ideality are present, as shown for example by Schaeffer et al.[55] Pyykkö,[56] and Prencipe et al.[57] In many cases, the T_m of a mixture is reported only at a specific mole ratio without confirmation that this is the eutectic temperature, and melting curves in solid−liquid phase diagrams are not available for most DESs studied. In addition, the measurement of melting curves has shown that cocrystals can form at certain molar ratios in some cases.[58,59]

The Schroeder−Van Laar equation also shows that T_m is influenced by pure component properties and intermolecular interactions in the mixture. Stronger hydrogen bonding in a DES tends to lower T_m, while increasing chain length enhances London dispersion forces and decreases hydrogen bonding, raising T_m. In DESs with straight-chain fatty acids, adding more constituents or longer chains disrupts crystalline order, reducing T_m.[60]

3.2. Heat of Fusion of DESs. $\Delta_{fus}h$ is a cornerstone property for materials used in TES, particularly in systems using PCMs. It determines the ability to store energy during phase transitions, such as melting or solidification, without a change in temperature. Combining high $\Delta_{fus}h$ with high density increases energy density of the PCM and consequently also the compactness and efficiency of TES systems.

There is a significant relationship between the HBA and HBD properties and the Δ_{fus}h values of DESs (Table S1). The $\Delta_{fus}h$ of a DES can be approximated as the sum of the energetic contributions arising from the disruption of hydrogen bonds and weaker van der Waals interactions between its constituents, expressed as eq 5.[61]

$$\Delta_{fus}h = \sum_i n_i \Delta H_{HB,i} + \Delta H_{vdW} \tag{5}$$

where n_i represents the number and strength of hydrogen bonds of type i, respectively, and $\Delta H_{HB,i}$ represents the enthalpy per hydrogen bond, and ΔH_{vdW} accounts for the van der Waals interactions present in the system. This equation reflects how breaking strong H-bonds alongside weaker nonspecific interactions underlies observed thermal transitions and T_m depression in DESs.[62]

T_m and $\Delta_{fus}h$ of DES mixtures depend critically on their proximity to the eutectic composition. Rather than being related to "enrichment" of a particular component, the T_m increases as the mixture deviates from the eutectic ratio, with the lowest T_m and characteristic sharp melting occurring exactly at the eutectic point where both components crystallize simultaneously.

To accurately quantify the $\Delta_{fus}h$ values of eutectic mixtures, Tamman plots are a valuable analytical tool. These plots represent $\Delta_{fus}h$ as a function of mixture composition and reveal linear trends on either side of the eutectic composition, which intersect at the eutectic point. This intersection allows the precise determination of both the eutectic $\Delta_{fus}h$ and the eutectic composition itself. Such analyses, as illustrated in Figure 9, are essential for understanding and optimizing the thermal properties of DESs for TES applications.

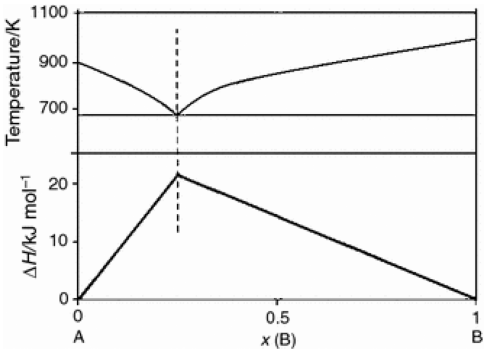

Figure 9. Tamman plot of a typical eutectic phase diagram. Reprinted with permission from ref 63. Copyright 2016 Springer Nature Link.

Figure 10 illustrates various types of PCMs, highlighting their dependence on T_m. Molten salts have the highest $\Delta_{fus}h$

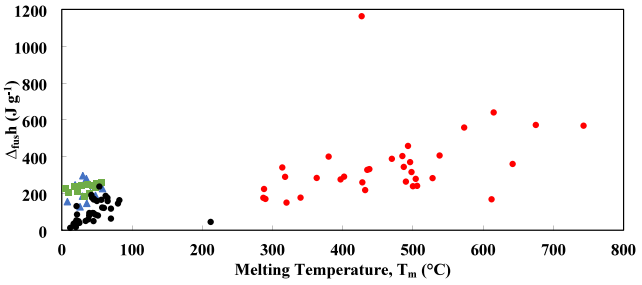

Figure 10. Enthalpy of fusion ($\Delta_{fus}h$) as a function of T_m for different types of PCMs. Salt hydrates are shown in blue triangles, organic PCMs in green squares, and composites in black circles, while molten salts are shown in red circles. The data is compiled from multiple literature sources.

but are suitable for high-temperature applications and are actively being used. Salt hydrates, paraffins, and composites lie in the same temperature window, with paraffins having higher $\Delta_{fus}h$ among the three.

Eutectic PCMs have a wide range of T_m, typically spanning from near ambient (0 °C) to around 60 °C. With further research and formulation, this range can be extended below 0 °C and beyond 100 °C. Eutectic PCMs (Figure 11) have relatively high $\Delta_{fus}h$ values, comparable to or exceeding those

https://doi.org/10.1021/acsaem.5c02743
ACS Appl. Energy Mater. XXXX, XXX, XXX−XXX

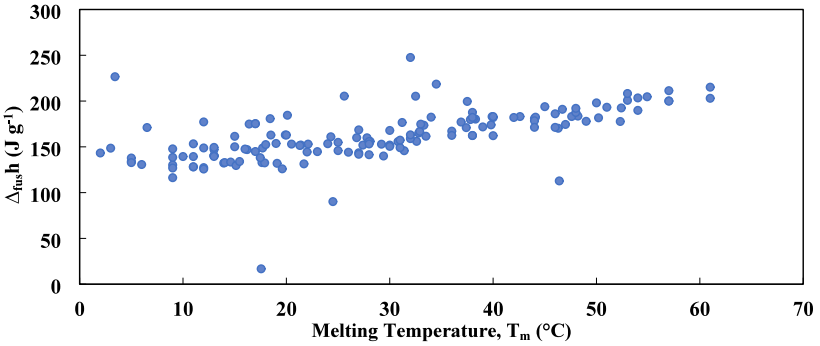

Figure 11. $\Delta_{fus}h$ as a function of T_m for different types of eutectic PCMs. Data are taken from Table S1.

Table 2. Decomposition Temperature Ranges of DES Families Are Dependent on the Type of HBD Precursor

HBD type	examples	decomposition temp. range	justification
sugars & polyols	glucose, xylitol, pentaerythritol	high (>160 °C)	strong H-bonding due to multiple −OH groups
carboxylic acids	adipic, succinic, formic acid	variable (≈50−≈230 °C)	smaller organic acids with very low decomposition temperature; more −COOH groups increase stability
ureas & thioureas	urea, thiourea, *N*-methylurea	moderate (≈130−≈200 °C)	higher stability with thiourea derivatives
amides	acetamide, *N*-methylacetamide	low (≈75−≈100 °C)	weak H-bonding
effect of HBA	allyl triphenyl phosphonium bromide (ATTPB) vs ChCl	ATTPB: high (>200 °C)	bulky structure and strong interactions

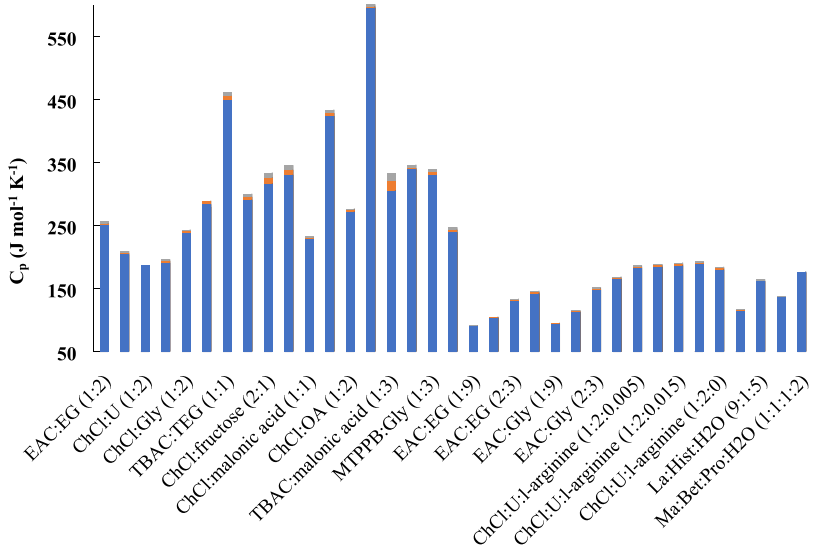

Figure 12. C_p of DESs at different temperatures. Blue bars represent $C_{p\ at}$ 30 °C, orange bars represent C_p at 40 °C, and gray bars represent C_p at 50 °C.

of organic PCMs. Because of their $\Delta_{fus}h$ and adaptability, they can be used in a variety of industries, including industrial heat recovery systems, solar TES, and building materials for passive heating and cooling. In addition, their ability to maintain precise temperatures during phase transitions makes them useful in sensitive applications such as biomedical storage and pharmaceutical cold chain logistics.

3.3. Thermal Stability and Reliability of DESs. The successful use of the LHTES system is heavily dependent on the thermal stability and reliability of the PCM used. The thermal reliability of a PCM is assessed by examining the changes in its LHTES properties after numerous melting and freezing cycles. Meanwhile, the thermal stability of a PCM refers to the highest temperature it can tolerate before decomposition, which is typically assessed by using thermogravimetric analysis (TGA). There are some studies on the thermal reliability of DESs. For example, Sari et al.[64] tested the LA:MA, LA:PA, and MA:SA for 1460 repeated cycles of melting and freezing and reported the −0.31, −0.40, and −1.11 °C change in T_m while 2.3, 1.1, and 0.9% change in $\Delta_{fus}h$. In another test, Sari et al.[65] tested DESs of LA:SA, MA:PA, and LA:PA for 360 cycles and observed changes in T_m within 1 °C and −6.2, −7.2, and 2.2% change in $\Delta_{fus}h$.[66] In an accelerated thermal cycling test of CA:PA with 5000 thermal cycles, an increase in T_m from 21.85 to 22.28 °C was measured and a drop from 173.16 to 161.26 J g^{-1} after 2000 cycles. After 5000 cycles, $\Delta_{fus}h$ increased to 175.02 J g^{-1}.[66]

https://doi.org/10.1021/acsaem.5c02743
ACS Appl. Energy Mater. XXXX, XXX, XXX−XXX

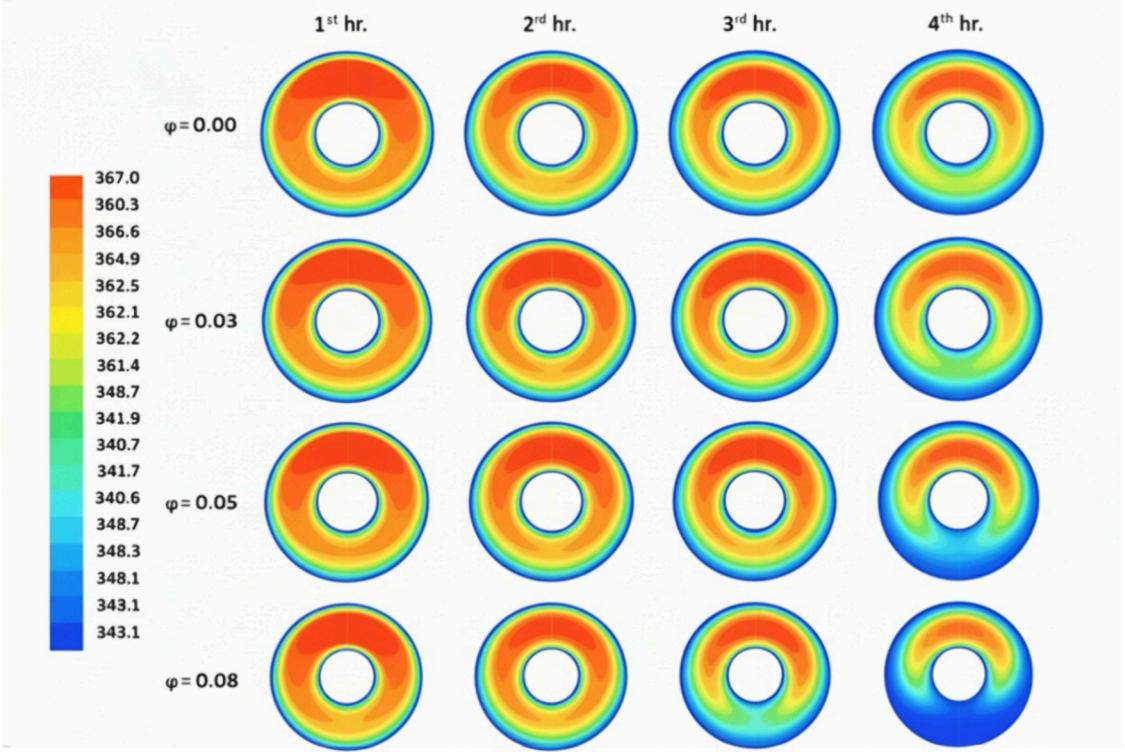

Figure 13. Distribution of isotherms at various time periods and various volume fractions (φ) of nanoparticles during the solidification of the nano-PCM (a paraffin-based PCM, RT82) at 70 °C. Reprinted with permission from ref 71. Copyright 2016 Elsevier.

Further details of the thermal reliability data are given in Table S2. The analysis shows that no eutectic PCM suffered from severe thermal reliability issues when subjected to repeated cycling. However, no studies have been conducted that extended beyond 10,000 thermal cycles. Ningbo Passive Edge Material Co., Ltd., a member of the RAL PCM quality association, a global network of leading PCM companies, classifies PCMs into grades ranging from A (10,000 cycles) to F (50 cycles), which reflects performance, quality, and reliability.[67] While this grading system provides a convenient framework for comparing PCM products, the company does not explicitly define the criteria for long-term industrial applicability.

Depending on the precursors of the DES, it could be thermally stable up to a certain temperature. Chen et al.[68] compared the thermal stability of different DESs. For example, they compared HBAs with various anions (ChCl, ChBr, and ChI) and found that due to its greater electronegativity, ChCl forms stronger hydrogen bonds with HBDs. Consequently, ChCl-based DESs decompose at higher temperatures than ChBr-based DESs, which are more stable than ChI-based DESs.

A comparison of the effect on DES degradation with respect to HBD is shown in Table 2. These results suggest that the choice of HBD, especially those with longer alkyl chains, plays a significant role in improving the thermal stability of DESs. In addition, it has been found that the thermal stability of DES decreases as the amount of HBD within the DES increases.[69] Furthermore, their stability over varying temperatures, as evident in the data, makes them ideal for applications involving cyclic heating and cooling.

3.4. Specific Heat Capacity of DESs. Simply put, C_p is the amount of energy required to raise the temperature of a unit mass or mole of material by one degree. C_p is a critical property in the design of the best possible LHTES system and is also used in determining thermophysical properties, such as the thermal diffusivity of the PCMs. When the thermal study of PCMs for LHTES is conducted, C_p is often overlooked. As a result, engineers must rely on estimates and simplified design assumptions, which can compromise system performance and efficiency. Figure 12 presents the C_p values of various eutectic mixtures.

There is significant variation in the C_p values among the different DESs. Since C_p is directly related to the thermodynamic degrees of freedom of a system, DESs composed of precursors with greater molecular complexity (e.g., large alkyl chains, several functional groups, etc.) tend to exhibit higher C_p values. For example, tetrabutylammonium chloride (TBAC):U (4:1) has an average C_p of 601 J mol^{-1} K^{-1} in the temperature range of 30−50 °C,[69] making it highly effective for sensible heat storage in high-demand applications like solar thermal power plants and waste heat recovery. Similarly, TBAC:TEG (1:1) shows a high average C_p of 455.60 J mol^{-1} K^{-1} over the same temperature range.[69] These high C_p values not only enhance energy storage efficiency but also reduce the volume of material required, contributing to cost savings and more compact, sustainable TES systems.

Detailed data on the C_p of various DESs are presented in Table S3. This data set underscores the potential of tailoring molar C_p values in DESs to meet a wide range of TES requirements, positioning them as innovative and adaptable materials for advancing TES technology. Notably, compounds with high degrees of freedom are often solid at room temperature, due to large molecular weights and strong intermolecular interactions. This characteristic represents a significant advantage for DESs in TES applications, as it

https://doi.org/10.1021/acsaem.5c02743
ACS Appl. Energy Mater. XXXX, XXX, XXX−XXX

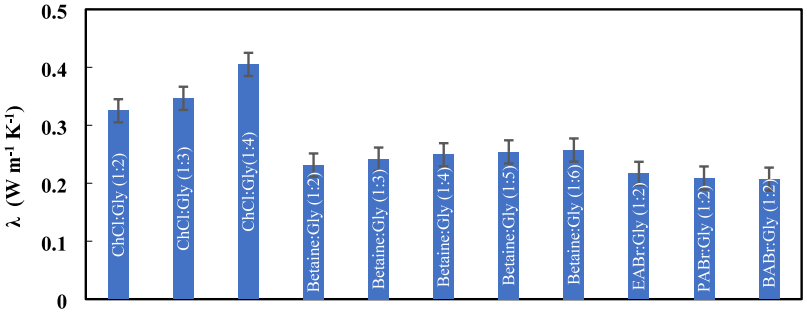

Figure 14. λ as a function of the molar ratio of Gly with different HBAs at 25 °C.

enables high energy storage densities while maintaining structural stability.

3.5. Thermal Conductivity of DESs. A higher λ value enhances the rate of heat transfer, leading to faster charging and discharging cycles. It can be visualized by Figure 13.

Measured λ values for different DES range from 0.045 to 0.423 W m^{-1} K^{-1} (Table S4). The increase in λ is attributed to the increased mobility and interaction of the molecules in the DES. For example, ChCl:Gly mixtures show higher λ at higher HBD ratios, from 0.32 W m^{-1} K^{-1} at a 1:2 ratio to 0.405 W m^{-1} K^{-1} at a 1:4 ratio (see Figure 14). A similar pattern is observed for DESs such as ChCl:EG (Figure 15) and

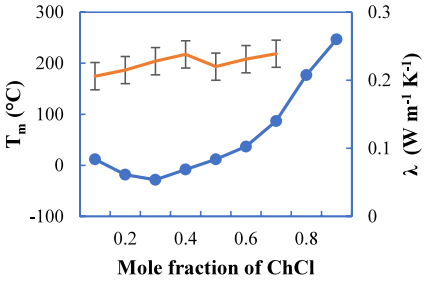

Figure 15. λ of the ChCl:EG as a function of T_m (°C) vs composition, blue markers represent T_m; orange line represents λ (data compiled from multiple literature sources; Table S4).

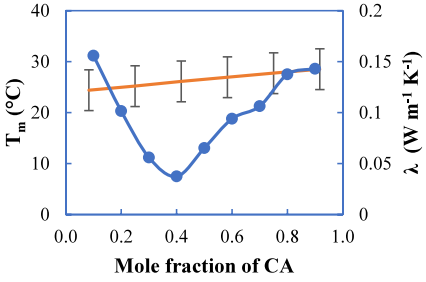

Figure 16. λ of the mixture of Capric acid and Menthol as a function of T_m (°C) vs composition; blue markers represent T_m, orange line represents λ (data taken from ref 75).

menthol:CA (Figure 16). It is important to note that the thermal conductivity of a DES closely follows that of its pure precursors. A higher λ in the pure components directly translates to a higher λ in the mixture. The role of hydrogen bond networks and ion interactions (e.g., Cl$^-$ with hydroxyl groups) is secondary to this effect, though they modulate thermal pathways.

In ChCl:OA and ChCl:MetA, λ decreases as the HBD ratio increases, likely due to increased viscosity. However, adding Gly and EG reduces the viscosity of DESs.[72,73] Hydrogen bonding networks influence λ, with bulky molecules such as CA and menthol limiting molecular interactions and thereby lowering the heat transfer efficiency. Smaller molecules such as Gly, U, and EG result in higher λ (see Figure 12) due to stronger hydrogen bonding and better packing. Overall, structural compactness and hydrogen bonding are key factors affecting thermal conductivity in DESs, as supported by a recent review.[73]

λ of DESs containing Gly is directly related to the ratio of Gly in the DES (Figure 14). A similar trend is observed in HBA:EG mixtures, with a few exceptions. DES, with higher ChCl ratios, shows more stable values. The higher λ in type I and II DES (Table S3) could also be related to the type of structure ions, such as Na^+, K^+, Cl^-.[74] The increasing proportion of the smaller components, which improve molecular alignment and strengthen hydrogen bonding networks, facilitates improved heat transfer by increasing λ.

The effect of composition on λ is seen in Figures 15 and 16.

Temperature has a relatively minor effect on the λ values of some DESs. For example, the conductivity of ChCl:U (1:2) decreases only slightly with increasing temperature, from 0.245 W m^{-1} K^{-1} at 25 °C to 0.244 W m^{-1} K^{-1} at 30 °C. This subtle change suggests that temperature has an effect on molecular mobility and hydrogen bonding network stability. However, the reliability of such data is questionable, as reported λ values for the same DES vary up to 30% across different studies.[74,76−79] Typically, λ decreases with increasing temperature, but some DESs, such as malic acid: glycine and Gly:proline mixtures, deviate from this trend. This behavior has been attributed to the presence of adsorbed water.[74] Interestingly, pure Gly also shows the same behavior, i.e. its λ increases with temperature, similar to water.[80] However, this behavior is not consistently observed across all Gly-based DESs, as shown in Figure 14.

3.6. Viscosity of DESs. Viscosity influences the process of LHTES storage by affecting the efficiency of heat transfer. It also affects nucleation and crystal growth processes, thereby impacting the rate at which the $\Delta_{fus}h$ is released.[81,82] However, predicting viscosity across a wide range of DES compositions is challenging, as these systems are typically nonideal. Simple mixing rules often fail, as demonstrated in other nonideal mixtures. For example, Jun Cao et al.[83] designed two series of DESs, one based on ChCl and the other on menthol, combined with HBDs such as 1-propanol, propionic acid, propionamide, L-alanine, propylamine, EG, polyethylene glycol (PEG), Gly, xylitol, mannitol, sorbitol, acetic acid (AC), butyric acid, hexanoic acid (HA), OA, malonic acid, succinic

https://doi.org/10.1021/acsaem.5c02743
ACS Appl. Energy Mater. XXXX, XXX, XXX−XXX

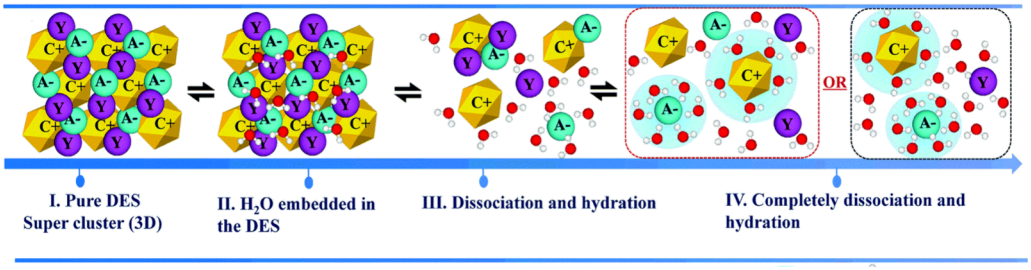

Figure 17. General schematic mechanism for the typical DES−H_2O systems. Note, the yellow, blue, red, and purple ones represent cation, anion, H_2O and HBD, respectively. Reprinted with permission from ref 94. Copyright 2018 The Royal Society of Chemistry.

acid, 2-HPA, U, methyl urea, and hydroxy urea. These DESs exhibited a wide range of densities and viscosities, as summarized in Table S5. Similarly, Cotroneo-Figueroa et al.,[84] synthesized a series of ChCl-based DESs with EG, 1,3-propanediol (1,3-PDO), and 1,4-butanediol (1,4-PDO) in various ratios, further highlighting the compositional sensitivity of viscosity in DES systems.

The viscosity of DESs with ChCl as the HBA and glycols as the HBD is strongly influenced by the chain length of the glycols. ChCl:EG (1:2) has a viscosity of 48 mPa s^{-1} at 25 °C. However, adding one ethylene unit to the glycol increases the viscosity to 150 mPa s^{-1}, with further increases observed as the chain length grows. This trend is primarily attributed to the inherent viscosity of the pure glycols, which rises with the molecular size due to stronger van der Waals interactions. The increase is not necessarily a result of stronger hydrogen bonding with ChCl. Additionally, longer chains also lead to greater molecular entanglement, contributing to the increased resistance to flow in the DES.

Strong electrostatic interactions between chloride ions (Cl^-) and HBD contribute to increased viscosity in DESs. The inclusion of higher glycols can mitigate this effect by acting as plasticizers and lubricants. Gly chains containing methyl groups, such as 1,2-PDO (72 mPa s^{-1} at 25 °C) and 1,4-BDO (87 mPa s^{-1}), increase viscosity.[71] In general, HDES exhibit viscosities lower than those of their hydrophilic counterparts, primarily because they possess fewer hydrogen bonding sites.

The choice of HBAs also influences the viscosity of the DESs. For example, the viscosities of ChCl:MEA, TBAB:MEA, and MTPPB:MEA, are 48.50, 106.5, and 128.9 mPa s^{-1}, respectively.[84] The literature suggests that DESs composed of smaller, less complex, and nonpolar components tend to exhibit lower viscosities compared to those formed with larger, more structurally complex molecules containing multiple polar functional groups. This highlights the tunability of DES properties through the careful selection of precursors.

3.7. Density and Thermal Expansion of DESs. While the relationship between the $\Delta_{fus}h$ and the substance's density is not direct, both properties are influenced by molecular interactions and intrinsic material characteristics. Notably, density plays a key role in determining a material's capacity to store latent and sensible heat per unit volume. However, we emphasize latent heat. A denser material can hold more thermal energy per unit volume, as long as $\Delta_{fus}h$ does not decrease significantly, according to eq 6.

$$Q = m\Delta_{fus}h \tag{6}$$

where Q is the stored heat and m is the mass of the material.

Most DESs have densities ranging from 0.9 to 1.5 g cm^{-3} within the temperature range of 20 to 60 °C (see Table S6). In comparison, the densities of common organic PCMs are generally lower: fatty acids ≈ 0.85−0.95 g cm^{-3}, fatty alcohols ≈ 0.82−0.85 g cm^{-3}, paraffins ≈ 0.78−0.83 g cm^{-3}, sugar alcohols ≈ 1.45−1.5 g cm^{-3}, and PEG polymers ≈ 1.2 g cm^{-3}. The density of DES is primarily determined by the densities of precursors, with cross/component hydrogen bonding playing a secondary role. An increase in H-bonding reduces free volume within the mixture, leading to higher density and vice versa.[85] For example, shorter diols tend to have lower densities than larger diols, a trend that extends to diol-based DESs: at 25 °C, ChCl: EG has a density of 1.119 g cm^{-3}, ChCl: 1,2-PDO 1.107 g cm^{-3}, and ChCl: 1,4-BDO 1.105 g cm^{-3}.[86] The HBD:HBA mole ratio also influences the DES density. Trichloroacetic acid (TCA), a very strong HBD with a high pure-component density (1.63 g cm^{-3}), forms one of the densest DES with ChCl (1.4662 g cm^{-3} at 20 °C). The second major factor affecting the densities is the temperature.

Given that the focus of this work is on LHTES, the densities of DESs do not significantly affect the amount of energy stored. However, less dense DESs require more space to store the PCM.

3.8. Impact of Water Additives On DES Properties. Water is widely regarded as one of the most effective TES materials due to its high C_p and $\Delta_{fus}h$. Its large $\Delta_{fus}h$ of 334 J g^{-1} at 0 °C makes it the lowest-temperature PCM among commonly used PCMs, and it naturally functions as a PCM in environmental systems. Interestingly, most DESs have C_p values that exceed that of water in J mol^{-1} (see Table S3). Therefore, the addition of water can reduce the C_p of DESs, as shown by Naser et al.[70] They reported that the C_p of TBAC:Gly, TBAC:TEG, and TBAC:EG decreased from 281 to 187, 445 to 272, and 288 to 175 J mol^{-1} K^{-1}, respectively, upon 50% water addition at 25 °C. A similar trend was reported by Siongco et al.[87]

The presence of water also influences other physicochemical properties critical to TES. For example, it enhances λ of DESs due to increased molecular mobility and efficient heat transfer properties of water molecules which improves their ability to efficiently transfer heat in systems such as TES or heat transfer fluids.[88,89] In the DES ChCl:EG (1:5, 1:6, 1:7, 1:8), λ increases linearly from 0.22, 0.231, 0.239, and 0.245 W m^{-1} K^{-1} to 0.274, 0.271, 0.272, and 0.271 W m^{-1} K^{-1} with up to 14.4% water addition.[90] Similar enhancements have been reported by Ibrahim et al.[76] for six ChCl-based DESs. Moreover, water affects phase transition temperatures such as melting or freezing point, necessitating precise control to maintain compatibility with operating temperature ranges.[91,92] For example, the T_m of ChCl:U (1:2), a hydrophilic DES,

https://doi.org/10.1021/acsaem.5c02743
ACS Appl. Energy Mater. XXXX, XXX, XXX−XXX

decreases linearly with increasing water content. In TBAC-CA DES the main endothermic peak shifts downward by approximately 10 °C for every 0.1 increase in water mole fraction.[87] Controlling the water content is therefore essential for ensuring the stability and durability of DESs in thermal applications. Spectroscopic studies by Gabriele et al.[93] and Castro et al.[94] have shown that water weakens the H-bonding between HBA and HBD, reducing structural integrity. Excessive water can trigger unwanted chemical reactions, such as hydrolysis, compromising the long-term performance of the TES system. Furthermore, weakened H-bonding may lead to phase separation (see Figure 17), further limiting the applicability of DESs in TES systems.

Elevated water content in DESs can induce undesirable effects such as cold crystallization[90] and affect the important parameters like C_p, λ and T_m which directly impact the energy storage capacity and efficiency of PCM in thermal systems.[95] Therefore, careful control of water content is essential to optimize the thermal properties, stability, and overall performance of DESs in various thermal applications.

3.9. Effect of Nanomaterials and Other Additives on PCM. The performance of DESs in TES applications can be significantly changed by the addition of nanoparticles (NPs), which are well-known for their exceptional dispersibility and thermal properties. These nanoenhanced DESs (NP-modified DESs) are expected to find applications in engineering applications such as solar thermal fluids,[96] thermal storage systems,[97] and as cooling/heating agents in industrial plants, machinery, electronics, or metallurgical processes,[98−101] as well as various other thermal management systems.[102] The addition of NPs improves the efficiency of energy storage and release by optimizing the heat conduction pathways within the DES matrix. Some NPs, such as carbon-based materials or metal oxides, can also enhance the C_p of DES, thereby improving their overall energy storage capacity.[103] According to Mahmud,[104] NPs can help prevent phase separation and degradation of DES components, contributing to improved system reliability and extended operational lifetime. Moreover, the tunability of NPs modified DES allows for precise tailoring of properties to meet the specific requirements of TES applications.

Polymer encapsulation has proven to be effective in suppressing supercooling in PCMs. Rajagopalan and Sukhishvili[105] showed that Diels−Alder cross-linked salogels, synthesized from furan-modified poly(vinyl alcohol) and bismaleimide polyethylene glycol (F10-PVA/BM-PEG), can stabilize salt hydrate PCMs across a range of temperatures. Their study showed a reduction in supercooling by 31 °C for lithium nitrate trihydrate (LNH) and 17 °C for magnesium nitrate hexahydrate (MgNH). This strategy may be expandable to other salt hydrates and organic PCMs, provided suitable polymer/furan modifications are employed (Figure 18).

Seeding is another effective strategy for reducing supercooling and phase segregation in DES-based TES systems. This method involves introducing a nucleating agent, typically an impurity, to promote crystallization. Shahbaz et al.[106] investigated this approach by adding fumed silica as a nucleating agent to a DES formulation labeled as DES4 (ChCl: $CaCl_2.H_2O$, X_{ChCl} = 0.11). Their results demonstrated an average supercooling reduction to just 1.23 °C over 100 thermal cycles, along with a stable T_m and significantly reduced phase segregation (Figure 19).

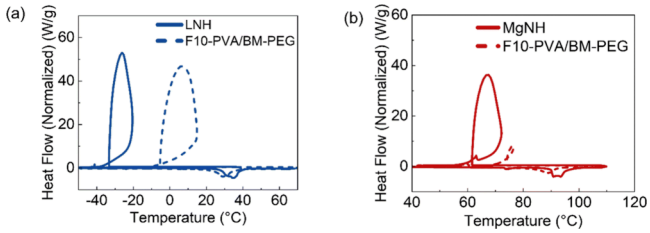

Figure 18. Differential scanning calorimetry thermograms show melting and crystallization transitions in (a) neat LNH and DA salogel and (b) neat MgNH and DA salogels. Comparison of the $\Delta_{fus}h$ and T_m in the DA salogel in (c) LNH and (d) MgNH before and after thermal cycling. These experiments were performed with a few grams of DA salogel sealed in a glass vial. Reprinted with permission from ref 105. Copyright 2025 The Royal Society of Chemistry.

Significant improvements in λ and C_p have been observed in phosphonium-based DESs upon the dispersion of alumina NPs, outperforming several commercial HTFs.[107] The thermal performance and stability of DESs in TES systems can be finely tuned by selecting NPs with desired properties, such as particle size, shape, and surface chemistry.[108,109] At a NP loading of just 0.005 vol %, Dehury et al.[110] reported enhancement of 50% in C_p and 24% in λ, demonstrating the potential of NP-modified DESs for high-efficiency TES.

As PCM changes nucleation sites, NPs dispersed throughout DES can accelerate phase transitions and improve the effectiveness of energy storage. Chen et al.[111] reported that carbon nanotubes (CNT) dispersion improved the kinetic properties, activation energies, and thermal stability of DESs.

3.10. Use of Machine Learning. The vast number of DES formulations and the factors affecting their properties make experimental evaluation impractical. Machine learning (ML) provides a practical and powerful way to efficiently identify the most suitable DESs for targeted application. In the past, traditional models such as support vector machines (SVM), and artificial neural networks (ANN) have extensively been used for quantitative structure property relationship (QSPR) analysis, empirical property prediction, and classification tasks owing to their interpretability and robust performance on moderate-sized data sets.

Today, the integration of high-throughput computational screening, ML, and physics-based models is enabling the development of autonomous materials discovery platforms. As the field develops, these hybrid ML frameworks are expected to become standard tools for the rational design of DESs, providing both efficiency and valuable insights to supplement traditional experimental methods.

Future developments of ensemble models like XGBoost,[112] random forests (RF),[113] especially when combined with active learning, promise autonomous discovery platforms capable of identifying DESs from non-DESs tailored for specific temperature ranges. The combination of Conductor-like Screening Model for Real Solvents (COSMO-RS) with models such as Neural Network Multilayer Perceptrons and SVM could be helpful in predicting C_p of DESs. Models such as feedforward neural networks and Gaussian Process Regression, utilizing COSMO-RS-derived sigma profiles interpretability aided by SHapley Additive exPlanations (SHAP) analysis,[114] offer a powerful tool for property prediction.[115]

Furthermore, hybrid frameworks that couple ML with physics-based models (e.g., PC-SAFT or COSMO-RS) improve both interpretability and generalizability of predic-

https://doi.org/10.1021/acsaem.5c02743
ACS Appl. Energy Mater. XXXX, XXX, XXX−XXX

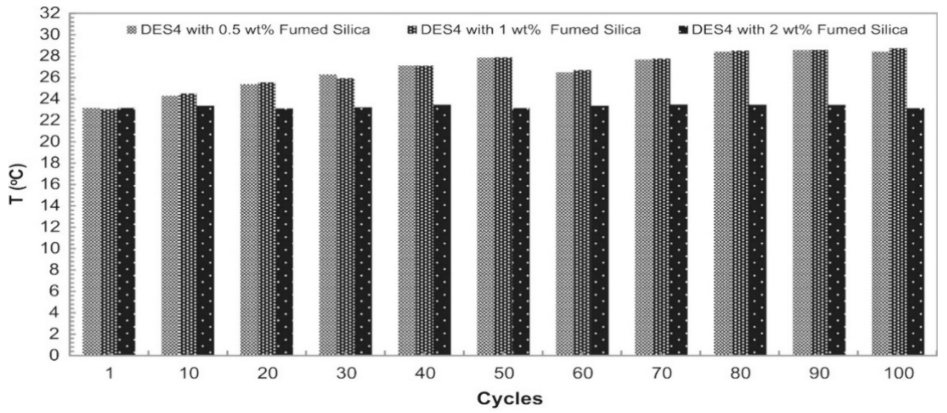

Figure 19. Phase change temperature of DES4 with the nucleating agent during 100 cycles (uncertainty in data was not reported). Reprinted with permission from ref 106. Copyright 2016 The Royal Society of Chemistry.

tions, allowing reliable extrapolation beyond the training domain. By combining experimental data with data-driven predictions, these approaches can optimize the number of experiments, shorten development cycles, and accelerate the discovery and design of DESs for TES applications.

FUTURE PERSPECTIVES AND CONCLUSIONS

Despite their promising characteristics, the application of DESs in TES is limited by a lack of comprehensive thermophysical data. In contrast, molten salts and organic PCMs are relatively well studied, leaving a significant opportunity to explore new eutectic mixtures with improved $\Delta_{fus}h$, λ and stability. In addition, eutectics could be combined with composites or advanced nanomaterials to enhance and tailor their performance for specific TES applications. DESs are particularly attractive as PCMs for TES applications due to their tunable properties, relatively simple preparation methods, and potential for customization. Key performance indicators include $\Delta_{fus}h$, T_m, thermal stability, and the influence of NPs as additives. Notably, DESs can exhibit high $\Delta_{fus}h$ values (e.g., a eutectic mixture of SA:1,10-decanediol stores 247 J g^{-1}, similarly SA:LA has 218 J g^{-1}) and sharp T_m values, which are critical for efficient TES and release. Additionally, DESs benefit from low thermal expansion, enabling high energy density per unit mass and offering advantages over conventional organic PCMs in TES systems.

The T_m of DESs can be precisely tuned by choosing appropriate HBAs and HBDs, allowing for customization for specific temperature needs. DESs also demonstrate excellent thermal stability across multiple thermal cycles, ensuring long-term reliability in TES systems. Their λ values generally range from 0.18 to 0.4 W m^{-1} K^{-1}, often exceeding that of many organic compounds. This property is influenced by factors like hydrogen bonding, molecular interactions, and the presence of additives. Stronger hydrogen bonds tend to restrict molecular mobility, thereby lowering λ, while smaller molecules or hydroxyl groups can enhance heat transfer. However, variability in measurement results makes it challenging to establish consistent trends, highlighting the need for further systematic research to better understand and optimize the thermal behavior of DESs.

Future research should focus on identifying HBDs with strong intermolecular interactions, such as polyols, to promote more ordered premelting phases and enhance heat absorption. Investigating hydrophobic HBDs, including long-chain fatty acids, menthol, and thymol, could offer new pathways to increase $\Delta_{fus}h$ and reduce supercooling. Combining multiple HBDs and HBAs to form a ternary or quaternary DES may optimize molecular packing and further improve $\Delta_{fus}h$. Expanding data sets for λ and C_p under standardized conditions is essential for reliable comparisons and performance benchmarking. Systematic studies of HBA:HBD combinations are needed to establish correlations between the molecular structure and λ. Strategies such as adjusting HBA:HBD ratios, incorporating ionic or molecular additives, and designing novel HDES could enhance the performance of LHTES systems.

Although the eutectic PCMs have shown no significant changes in T_m and $\Delta_{fus}h$ upon thermal cycling up to 5000 thermal cycles, industrial-scale TES requires stability beyond 10,000 cycles. Thus, current data does not effectively prove long-term reliability. Therefore, future research should also focus on extended thermal cycling tests to evaluate the reliability and performance under realistic operating conditions.

To date, most research on DESs has been limited to laboratory-scale investigations, leaving questions about process scalability, operational stability, and industrial feasibility largely unaddressed. Bridging this gap through pilot-scale studies is essential for translating the promising properties of DESs into practical, real-world TES applications.

Standardizing testing methods would greatly enhance the reliability of the thermophysical data for DESs. Material standardization should mandate reporting the purity grade and supplier for all HBAs and HBDs. Accurate water content measurement using Karl Fischer titration is crucial, as water can significantly affect DES properties. For phase transition measurements with differential scanning calorimetry, researchers should use sealed pans to prevent evaporation and preserve the sample integrity. A standard thermal pretreatment, like 3 melt-freeze cycles, is recommended to ensure a consistent thermal history. Slow heating/cooling rates help to reduce thermal lag and improve accuracy. The reported T_m should be the onset temperature, and the integration limits for $\Delta_{fus}h$ should be clearly defined and documented.

It is also important to note that several previous studies have reported the thermophysical properties of DESs without including the associated measurement uncertainties. This omission limits the reliability and comparability of the reported data across different research efforts.

https://doi.org/10.1021/acsaem.5c02743
ACS Appl. Energy Mater. XXXX, XXX, XXX−XXX

ML screening is the best way to accelerate DES discovery and optimization. Hybrid frameworks, such as SVM, ANN, and COSMO-RS, enhance property prediction, reduce experimentation, and aid in DES design. Ensemble models such as XGBoost and RF, especially with active learning, will enable autonomous discovery for specific temperatures, shortening development cycles for next-generation DESs PCMs. Future research focusing on the aforementioned gaps will maximize the potential of DESs, translating into industrial-scale PCMs.

■ ASSOCIATED CONTENT

Data Availability Statement

No new data has been generated in this study. All data that support the findings of this study are included within the text and supplementary data file.

Supporting Information

The Supporting Information is available free of charge at https://pubs.acs.org/doi/10.1021/acsaem.5c02743.

$\Delta_{fus}h$, thermal reliability, λ, C_p, density, and viscosity data tables (PDF)

■ AUTHOR INFORMATION

Corresponding Author

Oliver Järvik − *Department of Energy Technology, Tallinn University of Technology, Tallinn 19086, Estonia;* orcid.org/0000-0001-8530-2582; Email: oliver.jarvik@taltech.ee

Authors

Nouman Rafique − *Department of Energy Technology, Tallinn University of Technology, Tallinn 19086, Estonia;* orcid.org/0009-0002-2573-8178

Mihkel Koel − *Department of Energy Technology, Tallinn University of Technology, Tallinn 19086, Estonia*

Dinis O. Abranches − *CICECO − Aveiro Institute of Materials, Department of Chemistry, University of Aveiro, Aveiro 3810-193, Portugal;* orcid.org/0000-0003-0097-2072

Complete contact information is available at: https://pubs.acs.org/10.1021/acsaem.5c02743

Author Contributions

The manuscript was written through contributions of all authors. All authors have given approval to the final version of the manuscript.

Notes

The authors declare no competing financial interest.

■ ACKNOWLEDGMENTS

This work was supported by the Estonian Research Council grant *PRG1784*. This work was also developed within the scope of the project CICECO-Aveiro Institute of Materials, UIDB/50011/2020 (DOI 10.54499/UIDB/50011/2020), UIDP/50011/2020 (DOI 10.54499/UIDP/50011/2020) & LA/P/0006/2020 (DOI 10.54499/LA/P/0006/2020), financed by national funds through the FCT/MCTES (PIDDAC).

■ ABBREVIATIONS

1,2-PDO, 1,2-propanediol; 1,3- PDO, 1,3-propanediol; 2-HPA, 2-hydroxypropanoic (lactic) acid; ANN, artificial neural networks; AP, 3-amino-1-propanol; AC, acetic acid; AeChCl, acetylcholinium chloride; ADA, adipic acid; ATPB, allyl triphenyl phosphonium bromide; AzA, azelaic acid; BeA, benzilic acid; BzChCl, benzyldimethyl(2-hydroxyethyl)-ammonium chloride; BTMA, benzyltrimethylammonium chloride; BTPC, benzyl triphenyl phosphonium chloride; BoA, boric acid; ChBr, choline bromide; COSMO-RS, conductor-like screening model for real solvents; CAA, chloroacetic acid; CNT, carbon nanotubes; ChCl, choline chloride; CA, decanoic (capric) acid; DES, deep eutectic solvents; DEA, diethanolamine; LA, dodecanoic (lauric) acid; EA, ethanolamine; EAC, ethanolamine chloride; EG, ethylene glycol; Gly, glycerol; Gua, guanidinium hydrochloride; $\Delta_{fus}h$ (J g^{-1}), heat of fusion; HTFs, heat transfer fluids; MrA, heptadecanoic (margaric) acid; PA, hexadecenoic (palmitic) acid; HA, hexanoic acid; HBA, hydrogen bond acceptor; HBD, hydrogen bond donor; LHTES, latent heat thermal energy storage; MetA, methylmalonic acid; LV, levulinic acid; ML, machine learning; MTPPB, methyl triphenyl phosphonium bromide; T_m (K), melting point; C_p (J K^{-1} mol^{-1}), molar heat capacity; MEA, monoethanol amine; MA, myristic acid; EAC, *N*,*N*−diethyl ethanol ammonium chloride; NPs, *N*anoparticles; NMA, *N*-methylacetamide; BHDE, *N*-Benzyl-2-hydroxy-*N*,*N*-dimethyl ethanaminium chloride; NDA, nonadecanoic acid; PgA, nonanoic (pelargonic) acid; OcA, octanoic acid; OeA, oleic acid; $(COOH)_2$, oxalic acid; PDA, pentadecanoic acid; PCM, phase change materials; PEG, polyethylene glycol; PT68, PureTemp 68; QSPR, quantitative structure property relationship; RF, random forests; SVM, support vector machines; SHAP, SHapley Additive exPlanations; SEA, sebacic acid; NaTFSI, sodium bis-(trifluoromethane)sulfonimide; SA, stearic acid; SUA, suberic acid; TEG, triethylene glycol; TCA, trichloroacetic acid; TBAB, tetrabutylammonium bromide; TBAHS, tetrabutylammonium hydrogen sulfate; TBAC, tetrabutylammonium chloride; TEACs, tetraethylammonium chloride; TEAB, tetraethylammonium bromide; TPAC, tetrapropylammonium chloride; TMAC, trimethylammonium chloride; TOPO, trioctylphosphine oxide; TPAB, tetrapropylammonium bromide; λ (W m^{-1} K^{-1}), thermal conductivity; TES, thermal energy storage; U, urea

■ REFERENCES

(1) Martins, M. A. R.; Pinho, S. P.; Coutinho, J. A. P. Insights into the Nature of Eutectic and Deep Eutectic Mixtures. *J. Solution Chem.* **2019**, *48*, 962−982.

(2) Omar, K. A.; Sadeghi, R. Physicochemical Properties of Deep Eutectic Solvents: A Review. *J. Mol. Liq.* **2022**, *360*, No. 119524.

(3) Coutinho, J. A. P.; Pinho, S. P. Special Issue on Deep Eutectic Solvents: A Foreword. *Fluid Phase Equilib.* **2017**, *448* (1), 1−1.

(4) Paiva, A.; Craveiro, R.; Aroso, I.; Martins, M.; Reis, R. L.; Duarte, A. R. C. Natural Deep Eutectic Solvents−Solvents for the 21st Century. *ACS Sustainable Chem. Eng.* **2014**, *2* (5), 1063−1071.

(5) Płotka-Wasylka, J.; de la Guardia, M.; Andruch, V.; Vilková, M. Deep Eutectic Solvents vs Ionic Liquids: Similarities and Differences. *Microchem. J.* **2020**, *159*, No. 105539.

(6) Perna, F. M.; Vitale, P.; Capriati, V. Deep Eutectic Solvents and Their Applications as Green Solvents. *Curr. Opin. Green Sustainable Chem.* **2020**, *21*, 27−33.

(7) Santana-Mayor, Á.; Rodríguez-Ramos, R.; Herrera-Herrera, A. V.; Socas-Rodríguez, B.; Rodríguez-Delgado, M. Á. Deep Eutectic Solvents. The New Generation of Green Solvents in Analytical Chemistry. *TrAC, Trends Anal. Chem.* **2021**, *134*, No. 116108.

(8) Deetlefs, M.; Seddon, K. R. Assessing the Greenness of Some Typical Laboratory Ionic Liquid Preparations. *Green Chem.* **2010**, *12* (1), 17−30.
(9) Abranches, D. O.; Coutinho, J. A. P. Everything You Wanted to Know about Deep Eutectic Solvents but Were Afraid to Be Told. *Annu. Rev. Chem. Biomol. Eng.* **2023**, *14* (1), 141−163.
(10) Singh, B. S.; Lobo, H. R.; Shankarling, G. S. Choline Chloride Based Eutectic Solvents: Magical Catalytic System for Carbon−Carbon Bond Formation in the Rapid Synthesis of β-Hydroxy Functionalized Derivatives. *Catal. Commun.* **2012**, *24*, 70−74.
(11) Haz, A.; Strižincová, P.; Majová, V.; Butor Skulcova, A.; Jablonsky, M. Thermal stability of selected deep eutectic solvents. *Int. J. Sci. Res.* **2016**, *7*, 14441−14444.
(12) van Osch, D. J. G. P.; Zubeir, L. F.; van den Bruinhorst, A.; Rocha, M. A. A.; Kroon, M. C. Hydrophobic Deep Eutectic Solvents as Water-Immiscible Extractants. *Green Chem.* **2015**, *17* (9), 4518−4521.
(13) Ribeiro, B. D.; Florindo, C.; Iff, L. C.; Coelho, M. A. Z.; Marrucho, I. M. Menthol-Based Eutectic Mixtures: Hydrophobic Low Viscosity Solvents. *ACS Sustainable Chem. Eng.* **2015**, *3* (10), 2469−2477.
(14) Dunlap, R. A. Sensible Heat Energy Storage. In *Renewable Energy Storage: Mechanical and Thermal Methods*; Springer Nature Switzerland: Cham, 2026; pp 67−89.
(15) Sharma, S. K.; Jotshi, C. K.; Kumar, S. Thermal Stability of Sodium Salt Hydrates for Solar Energy Storage Applications. *Sol. Energy* **1990**, *45* (3), 177−181.
(16) Bradshaw, R. W.; Meeker, D. E. High-Temperature Stability of Ternary Nitrate Molten Salts for Solar Thermal Energy Systems. *Sol. Energy Mater.* **1990**, *21* (1), 51−60.
(17) González-Roubaud, E.; Pérez-Osorio, D.; Prieto, C. Review of Commercial Thermal Energy Storage in Concentrated Solar Power Plants: Steam vs. Molten Salts. *Renewable Sustainable Energy Rev.* **2017**, *80*, 133−148.
(18) Bhatnagar, P.; Siddiqui, S.; Sreedhar, I.; Parameshwaran, R. Molten Salts: Potential Candidates for Thermal Energy Storage Applications. *Int. J. Energy Res.* **2022**, *46* (13), 17755−17785.
(19) Kearney, D.; Herrmann, U.; Nava, P.; Kelly, B.; Mahoney, R.; Pacheco, J.; Cable, R.; Potrovitza, N.; Blake, D.; Price, H. Assessment of a Molten Salt Heat Transfer Fluid in a Parabolic Trough Solar Field. *J. Sol. Energy Eng.* **2003**, *125* (2), 170−176.
(20) Caraballo, A.; Galán-Casado, S.; Caballero, Á.; Serena, S. Molten Salts for Sensible Thermal Energy Storage: A Review and an Energy Performance Analysis. *Energies* **2021**, *14* (4), 1197.
(21) Liu, J.; Yang, Y.; Li, A.; Wang, W.; Wu, W.; Zhang, H. Preparation and Assessment of a Novel Hydrated Salt PCM Applied for Intermittent Floor Radiant Heating Systems. *J. Energy Storage* **2025**, *105*, No. 114710.
(22) Brahimi, M. E.; Maliki, M.; Laredj, N.; Kuznik, F.; Sardou, M.; Missoum, H. Investigation of the Thermal Efficiency of Hollow Bricks Filled with Bio-Organic Phase Change Material Mixture. *J. Energy Storage* **2025**, *122*, No. 116667.
(23) Vighnesh, R.; Parol, V.; Anand, K. B. *Constr. Build. Mater.* **2025**, *490*, No. 142566.
(24) Hirschey, J.; Gluesenkamp, K. R.; Mallow, A.; Graham, S. Review of Inorganic Salt Hydrates with Phase Change Temperature in Range of 5°C to 60°C and Material Cost Comparison with Common Waxes. In *International High Performance Buildings Conference*; 2018. https://www.osti.gov/servlets/purl/1468092 (accessed 2025−10−28).
(25) Cabeza, L.; Heinz, A.; Streicher, W. *Inventory of Phase Change Materials (PCM)*. https://task32.iea-shc.org/Data/Sites/1/publications/task32-Inventory_of_PCM.pdf (accessed 2025−11−01).
(26) Duquesne, M.; Mailhé, C.; Doppiu, S.; Dauvergne, J.-L.; Santos-Moreno, S.; Godin, A.; Fleury, G.; Rouault, F.; Palomo del Barrio, E. Characterization of Fatty Acids as Biobased Organic Materials for Latent Heat Storage. *Materials* **2021**, *14* (16), 4707.
(27) Kulish, V.; Aslfattahi, N.; Schmirler, M.; Sláma, P. New Library of Phase-Change Materials with Their Selection by the Rényi Entropy Method. *Sci. Rep.* **2023**, *13* (1), 10446.
(28) Hirschey, J. R.; Kumar, N.; Turnaoglu, T.; Gluesenkamp, K. R.; Graham, S. Review of Low-Cost Organic and Inorganic Phase Change Materials with Phase Change Temperature between 0°C and 65°C. In *International High Performance Buildings Conference*; 2021. https://docs.lib.purdue.edu/ihpbc/389/ (accessed 2025−10−16).
(29) Duraipandi, S.; Somkunwar, S.; Appukuttan, S. Comprehensive Analysis of Thermophysical Properties of a Binary Stearyl Alcohol and Benzamide Eutectic Phase Change Material and Determination of Thermal Performance of a Solar Dryer Integrated with Phase Change Material. *Energy Storage* **2023**, *5* (7), No. e461.
(30) Duraipandi, S.; Sreekumar, A. Investigation on the Performance of a Natural Convection Solar Dryer with Novel Palmitic and Sebacic Acid Eutectic Phase Change Material for Thermal Energy Storage Applications. *J. Energy Storage* **2024**, *77*, No. 109908.
(31) O'Donnell, J.; von Bohrens, P. *Rondo*. https://www.rondo.com/how-it-works (accessed 2025−04−02).
(32) Sui, Y.; Ding, Z.; Zhai, C.; Lin, H.; Wu, W. Crystallization-Free and Low-Cost Deep Eutectic Solvents for Absorption Thermal Battery Utilizing Ultra-Low-Grade Energy. *Energy Convers. Manage.* **2023**, *284*, No. 116984.
(33) Peyrovedin, H.; Haghbakhsh, R.; Duarte, A. R. C.; Shariati, A. Deep Eutectic Solvents as Phase Change Materials in Solar Thermal Power Plants: Energy and Exergy Analyses. *Molecules* **2022**, *27* (4), 1427.
(34) Sui, Y.; Ding, Z.; Sui, Z.; Lin, H.; Li, F.; Wu, W. Seasonal Thermochemical Energy Storage with Affordable and High-Energy-Density Deep Eutectic Solvents. *Appl. Energy* **2025**, *386*, No. 125577.
(35) Du, K.; Calautit, J.; Wang, Z.; Wu, Y.; Liu, H. A Review of the Applications of Phase Change Materials in Cooling, Heating and Power Generation in Different Temperature Ranges. *Appl. Energy* **2018**, *220*, 242−273.
(36) Raj, V. A. A.; Velraj, R. Review on Free Cooling of Buildings Using Phase Change Materials. *Renewable Sustainable Energy Rev.* **2010**, *14* (9), 2819−2829.
(37) Butala, V.; Stritih, U. Experimental Investigation of PCM Cold Storage. *Energy Build.* **2009**, *41* (3), 354−359.
(38) Jani, A.; Sohier, T.; Morineau, D. Phase Behavior of Aqueous Solutions of Ethaline Deep Eutectic Solvent. *J. Mol. Liq.* **2020**, *304*, No. 112701.
(39) Umecky, T.; Yamaguchi, R.; Hashimoto, S.; Wakimoto, R.; Takeuchi, H. Stable Supercooling Formation of Guanidine Monohydrochloride-Based Deep Eutectic Solvent Induced by Monosubstitution of Urea as Hydrogen Bond Donor. *Phys. Chem. Liq.* **2024**, *62*, 491−499.
(40) Chang, S.-Y.; Sheng, Y.-J.; Tsao, H.-K. Abnormal Wetting Behavior of Supercooled Deep Eutectic Solvents. *J. Mol. Liq.* **2023**, *387*, No. 122617.
(41) Frukacz, Z.; Pawlak, D. A. Garnets, growth of. *Encycl. Mater.: Sci. Technol.* **2001**, 3455−3463.
(42) Mika, Ł.; Radomska, E.; Sztekler, K.; Gołdasz, A.; Zima, W. Review of Selected PCMs and Their Applications in the Industry and Energy Sector. *Energies* **2025**, *18* (5), 1233.
(43) Ona, E. P.; Zhang, X.; Kyaw, K.; Watanabe, F.; Matsuda, H.; Kakiuchi, H.; Yabe, M.; Chihara, S. Relaxation of Supercooling of Erythritol for Latent Heat Storage. *J. Chem. Eng. Jpn.* **2001**, *34* (3), 376−382.
(44) Zahir, Md. H.; Mohamed, S. A.; Saidur, R.; Al-Sulaiman, F. A. Supercooling of Phase-Change Materials and the Techniques Used to Mitigate the Phenomenon. *Appl. Energy* **2019**, *240*, 793−817.
(45) Zalba, B.; Marín, J. M.; Cabeza, L. F.; Mehling, H. Review on Thermal Energy Storage with Phase Change: Materials, Heat Transfer Analysis and Applications. *Appl. Therm. Eng.* **2003**, *23* (3), 251−283.
(46) Spietz, T.; Fryza, R.; Lasek, J.; Zuwała, J. Thermochemical Energy Storage Based on Salt Hydrates: A Comprehensive Review. *Energies* **2025**, *18* (10), 2643.

https://doi.org/10.1021/acsaem.5c02743
ACS Appl. Energy Mater. XXXX, XXX, XXX−XXX

(47) Zhou, D.; Zhao, C. Y. Experimental Investigations on Heat Transfer in Phase Change Materials (PCMs) Embedded in Porous Materials. *Appl. Therm. Eng.* **2011**, *31* (5), 970−977.
(48) Merlin, K.; Delaunay, D.; Soto, J.; Traonvouez, L. Heat Transfer Enhancement in Latent Heat Thermal Storage Systems: Comparative Study of Different Solutions and Thermal Contact Investigation between the Exchanger and the PCM. *Appl. Energy* **2016**, *166*, 107−116.
(49) Han, X. X.; Tian, Y.; Zhao, C. Y. An Effectiveness Study of Enhanced Heat Transfer in Phase Change Materials (PCMs). *Int. J. Heat Mass Transfer* **2013**, *60*, 459−468.
(50) Martínez, F. R.; Borri, E.; Mani Kala, S.; Ushak, S.; Cabeza, L. F. Phase Change Materials for Thermal Energy Storage in Industrial Applications. *Heliyon* **2025**, *11* (1), No. e41025.
(51) Richet, P. *The Physical Basis of Thermodynamics: With Applications to Chemistry*; Springer Science & Business Media: 2001.
(52) Bryant, S. J.; Christofferson, A. J.; Greaves, T. L.; McConville, C. F.; Bryant, G.; Elbourne, A. Bulk and Interfacial Nanostructure and Properties in Deep Eutectic Solvents: Current Perspectives and Future Directions. *J. Colloid Interface Sci.* **2022**, *608*, 2430−2454.
(53) Smith, E. L.; Abbott, A. P.; Ryder, K. S. Deep Eutectic Solvents (DESs) and Their Applications. *Chem. Rev.* **2014**, *114* (21), 11060−11082.
(54) Gilbert, M. Relation of Structure to Thermal and Mechanical Properties. In *Brydson's Plastics Materials*: Eighth Edition, Elsevier: **2017**, 59-73.
(55) Schaeffer, N.; Conceição, J. H. F.; Martins, M. A. R.; Neves, M. C.; Pérez-Sánchez, G.; Gomes, J. R. B.; Papaiconomou, N.; Coutinho, J. A. P. Non-Ionic Hydrophobic Eutectics−Versatile Solvents for Tailored Metal Separation and Valorisation. *Green Chem.* **2020**, *22* (9), 2810−2820.
(56) Pyykkö, P. Simple Estimates for Eutectic Behavior. *ChemPhysChem* **2019**, *20* (1), 123−127.
(57) Prencipe, M.; Mazzeo, P. P.; Bacchi, A. A Method to Predict Binary Eutectic Mixtures for Mechanochemical Syntheses and Cocrystallizations. *RSC Mechanochem.* **2025**, *2* (1), 61−71.
(58) Alhadid, A.; Jandl, C.; Mokrushina, L.; Minceva, M. Nonideality and Cocrystal Formation in L-Menthol/Xylenol Eutectic Systems. *J. Mol. Liq.* **2022**, *367*, No. 120582.
(59) Alhadid, A.; Jandl, C.; Mokrushina, L.; Minceva, M. Cocrystal Formation in Choline Chloride Deep Eutectic Solvents. *Cryst. Growth Des.* **2022**, *22* (3), 1933−1942.
(60) Ke, H. Phase Diagrams, Eutectic Mass Ratios and Thermal Energy Storage Properties of Multiple Fatty Acid Eutectics as Novel Solid-Liquid Phase Change Materials for Storage and Retrieval of Thermal Energy. *Appl. Therm. Eng.* **2017**, *113*, 1319−1331.
(61) Sokolov, A. A.; Solomonov, B. N.; Yagofarov, M. I. Hydrogen Bonding and van Der Waals Forces Contributions to the Melting Enthalpy: Insights from Volumetric and Spectroscopic Data. *Phys. Chem. Chem. Phys.* **2025**, *27*, 22196.
(62) Dimaano, M. N. R.; Watanabe, T. Performance Investigation of the Capric and Lauric Acid Mixture as Latent Heat Energy Storage for a Cooling System. *Sol. Energy* **2002**, *72* (3), 205−215.
(63) Dańczak, A.; Rycerz, L. Reinvestigation of the $DyCl_3$−LiCl Binary System Phase Diagram. *J. Therm. Anal. Calorim.* **2016**, *126* (1), 299−305.
(64) Sarı, A. Eutectic Mixtures of Some Fatty Acids for Low Temperature Solar Heating Applications: Thermal Properties and Thermal Reliability. *Appl. Therm. Eng.* **2005**, *25* (14), 2100−2107.
(65) Sarı, A.; Sarı, H.; Önal, A. Thermal Properties and Thermal Reliability of Eutectic Mixtures of Some Fatty Acids as Latent Heat Storage Materials. *Energy Convers. Manage.* **2004**, *45* (3), 365−376.
(66) Sarı, A.; Karaipekli, A. Preparation and thermal properties of capric acid/palmitic acid eutectic mixture as a phase change energy storage material. *Mater. Lett.* **2008**, *62* (6−7), 903−906.
(67) Gütesicherung Quality Assurance. *Quality and testing specifications for Phase Change Materials. Phase Change Materials.* https://pcm-ral.org/wp-content/uploads/2025/08/RAL-GZ-896_Phase-Change-Materials_August-2025.pdf (accessed 2025−10−22).
(68) Chen, W.; Xue, Z.; Wang, J.; Jiang, J.; Zhao, X.; Mu, T. Investigation on the Thermal Stability of Deep Eutectic Solvents. *Acta Phys. Chim. Sin.* **2018**, *34* (8), 904−911.
(69) Ghaedi, H.; Ayoub, M.; Sufian, S.; Hailegiorgis, S. M.; Murshid, G.; Khan, S. N. Thermal Stability Analysis, Experimental Conductivity and pH of Phosphonium-Based Deep Eutectic Solvents and Their Prediction by a New Empirical Equation. *J. Chem. Thermodyn.* **2018**, *116*, 50−60.
(70) Naser, J.; Mjalli, F. S.; Gano, Z. S. Molar Heat Capacity of Selected Type III Deep Eutectic Solvents. *J. Chem. Eng. Data* **2016**, *61* (4), 1608−1615.
(71) Mahdi, J. M.; Nsofor, E. C. Solidification of a PCM with Nanoparticles in Triplex-Tube Thermal Energy Storage System. *Appl. Therm. Eng.* **2016**, *108*, 596−604.
(72) Gajardo-Parra, N. F.; Cotroneo-Figueroa, V. P.; Aravena, P.; Vesovic, V.; Canales, R. I. Viscosity of Choline Chloride-Based Deep Eutectic Solvents: Experiments and Modeling. *J. Chem. Eng. Data* **2020**, *65* (11), 5581−5592.
(73) Wang, H.; Wang, Y.; Wang, S.; Li, H.; Peng, S.; Wang, Y.; Li, H.; Fang, J. Density and Viscosity of Deep Eutectic Solvents at Different Temperatures and Compositions: Measurement and Prediction Model. *Asia-Pac. J. Chem. Eng.* **2024**, *19*, No. e3035.
(74) Atilhan, M.; Aparicio, S. A Review on the Thermal Conductivity of Deep Eutectic Solvents. *J. Therm. Anal. Calorim.* **2023**, *148* (17), 8765−8776.
(75) Yu, L.-Y.; Hou, X.-J.; Wu, K.-J.; He, C.-H. Measurements of the Thermal Conductivity of l-Menthol−Decanoic Acid Deep Eutectic Solvents in the Temperature Range from 283.15 to 363.15 K at Pressures up to 15.1 MPa. *J. Chem. Eng. Data* **2021**, *66* (5), 2061−2070.
(76) Agieienko, V.; Buchner, R. Is Ethaline a Deep Eutectic Solvent? *Phys. Chem. Chem. Phys.* **2022**, *24* (9), 5265−5268.
(77) Ibrahim, T. H.; Sabri, M. A.; Abdel Jabbar, N.; Nancarrow, P.; Mjalli, F. S.; AlNashef, I. Thermal Conductivities of Choline Chloride-Based Deep Eutectic Solvents and Their Mixtures with Water: Measurement and Estimation. *Molecules* **2020**, *25* (17), 3816.
(78) Celebi, A. T.; Vlugt, T. J. H.; Moultos, O. A. Thermal Conductivity of Aqueous Solutions of Reline, Ethaline, and Glyceline Deep Eutectic Solvents; a Molecular Dynamics Simulation Study. *Mol. Phys.* **2021**, *119* (19−20), No. e1876263.
(79) Sander, A.; Rogošić, M.; Slivar, A.; Žuteg, B. Separation of Hydrocarbons by Means of Liquid-Liquid Extraction with Deep Eutectic Solvents. *Solvent Extr. Ion Exch.* **2016**, *34* (1), 86−98.
(80) Liu, C.; Fang, H.; Qiao, Y.; Zhao, J.; Rao, Z. Properties and Heat Transfer Mechanistic Study of Glycerol/Choline Chloride Deep Eutectic Solvents Based Nanofluids. *Int. J. Heat Mass Transfer* **2019**, *138*, 690−698.
(81) Sharifpur, M.; Tshimanga, N.; Meyer, J. P.; Manca, O. Experimental Investigation and Model Development for Thermal Conductivity of α-Al_2O_3-Glycerol Nanofluids. *Int. Commun. Heat Mass Transfer* **2017**, *85*, 12−22.
(82) Kumari, P.; Raj, A.; Ghosh, D. Selection of Phase Change Material for Latent Heat Thermal Energy Storage Using a Hairpin Heat Exchanger: Numerical Study. *J. Therm. Sci. Eng. Appl.* **2024**, *16* (9), No. 091005.
(83) Cao, J.; Zhu, F.; Dong, Q.; Wu, R.; Su, E. Insight into the Physicochemical Properties of Deep Eutectic Solvents by Systematically Investigating the Components. *J. Mol. Liq.* **2022**, *346*, No. 118315.
(84) Cotroneo-Figueroa, V. P.; Gajardo-Parra, N. F.; López-Porfiri, P.; Leiva, Á.; Gonzalez-Miquel, M.; Garrido, J. M.; Canales, R. I. Hydrogen Bond Donor and Alcohol Chain Length Effect on the Physicochemical Properties of Choline Chloride Based Deep Eutectic Solvents Mixed with Alcohols. *J. Mol. Liq.* **2022**, *345*, No. 116986.
(85) Peng, D.; Yu, Z.; Alhadid, A.; Minceva, M. Modeling the Viscosity of ChCl-Based Deep Eutectic Solvents and Their Mixtures with Water. *Ind. Eng. Chem. Res.* **2024**, *63* (3), 1623−1633.
(86) Basaiahgari, A.; Panda, S.; Gardas, R. L. Effect of Ethylene, Diethylene, and Triethylene Glycols and Glycerol on the

https://doi.org/10.1021/acsaem.5c02743
ACS Appl. Energy Mater. XXXX, XXX, XXX−XXX

Physicochemical Properties and Phase Behavior of Benzyltrimethyl and Benzyltributylammonium Chloride Based Deep Eutectic Solvents at 283.15−343.15 K. *J. Chem. Eng. Data* **2018**, *63* (7), 2613−2627.
(87) Siongco, K. R.; Leron, R. B.; Caparanga, A. R.; Li, M.-H. Molar Heat Capacities and Electrical Conductivities of Two Ammonium-Based Deep Eutectic Solvents and Their Aqueous Solutions. *Thermochim. Acta* **2013**, *566*, 50−56.
(88) Kivelä, H.; Salomäki, M.; Vainikka, P.; Mäkilä, E.; Poletti, F.; Ruggeri, S.; Terzi, F.; Lukkari, J. Effect of Water on a Hydrophobic Deep Eutectic Solvent. *J. Phys. Chem. B* **2022**, *126* (2), 513−527.
(89) Abbott, A. P.; Boothby, D.; Capper, G.; Davies, D. L.; Rasheed, R. K. Deep Eutectic Solvents Formed between Choline Chloride and Carboxylic Acids: Versatile Alternatives to Ionic Liquids. *J. Am. Chem. Soc.* **2004**, *126* (29), 9142−9147.
(90) Lan, T.; Xu, J.; Wang, C.; Wang, Y.; Liu, X.; He, M. The Effect of Water on the Thermal Conductivities of Deep Eutectic Solvents (Choline Chloride + Ethylene Glycol) Using Two-Wire Structure 3ω Method. *J. Mol. Liq.* **2022**, *359*, No. 119330.
(91) Meng, X.; Ballerat-Busserolles, K.; Husson, P.; Andanson, J.-M. Impact of Water on the Melting Temperature of Urea+ Choline Chloride Deep Eutectic Solvent. *New J. Chem.* **2016**, *40* (5), 4492−4499.
(92) Zhang, H.; Zhang, N.; Sun, Q.; Cao, X. Effect of Water Content on the Phase Transition Temperature, Latent Heat and Water Uptake of PEG Polymers Acting as Endothermal-Hydroscopic Materials. *J. Therm. Anal. Calorim.* **2016**, *126*, 699.
(93) Gabriele, F.; Chiarini, M.; Germani, R.; Tiecco, M.; Spreti, N. Effect of Water Addition on Choline Chloride/Glycol Deep Eutectic Solvents: Characterization of Their Structural and Physicochemical Properties. *J. Mol. Liq.* **2019**, *291*, No. 111301.
(94) Castro, A. M. de; Prasavath, D.; Bevilaqua, J. V.; Portugal, C. A. M.; Neves, L. A.; Crespo, J. G. Role of Water on Deep Eutectic Solvents (DES) Properties and Gas Transport Performance in Biocatalytic Supported DES Membranes. *Sep. Purif. Technol.* **2021**, *255*, No. 117763.
(95) Ma, C.; Laaksonen, A.; Liu, C.; Lu, X.; Ji, X. The Peculiar Effect of Water on Ionic Liquids and Deep Eutectic Solvents. *Chem. Soc. Rev.* **2018**, *47* (23), 8685−8720.
(96) Mitali, J.; Dhinakaran, S.; Mohamad, A. A. Energy Storage Systems: A Review. *Energy Storage Sav.* **2022**, *1* (3), 166−216.
(97) Dehury, P.; Upadhyay, A. K.; Banerjee, T. Evaluation and Conceptual Design of Triphenylphosphonium Bromide-Based Deep Eutectic Solvent as Novel Thermal Nanofluid for Concentrated Solar Power. *Bull. Mater. Sci.* **2019**, *42* (6), 262.
(98) Shafee, A.; Sheikholeslami, M.; Wang, P.; Selimefendigil, F.; Babazadeh, H. Phase Change Process of Nanoparticle Enhanced PCM in a Heat Storage Including Unsteady Conduction. *J. Mol. Liq.* **2020**, *309*, No. 113102.
(99) Selimefendigil, F.; Öztop, H. F. Effects of Using a Porous Disk on the Dynamic Features of Phase Change Process with PCM Integrated Circular Pipe during Nano-Liquid Forced Convection in Discharging Operation Mode. *J. Taiwan Inst. Chem. Eng.* **2021**, *124*, 381−390.
(100) Gautam, R. K.; Seth, D. Thermal Conductivity of Deep Eutectic Solvents. *J. Therm. Anal. Calorim.* **2020**, *140* (6), 2633−2640.
(101) Hajizadeh, M. R.; Selimefendigil, F.; Muhammad, T.; Ramzan, M.; Babazadeh, H.; Li, Z. Solidification of PCM with Nano Powders inside a Heat Exchanger. *J. Mol. Liq.* **2020**, *306*, No. 112892.
(102) Wu, J. M.; Zhao, J. A Review of Nanofluid Heat Transfer and Critical Heat Flux Enhancement—Research Gap to Engineering Application. *Prog. Nucl. Energy* **2013**, *66*, 13−24.
(103) Paul, T. C.; Morshed, A. K. M. M.; Fox, E. B.; Khan, J. A. Experimental Investigation of Natural Convection Heat Transfer of Al_2O_3 Nanoparticle Enhanced Ionic Liquids (NEILs). *Int. J. Heat Mass Transfer* **2015**, *83*, 753−761.
(104) Mahmud, M. Z. A. A Concise Review of Nanoparticles Utilized Energy Storage and Conservation. *J. Nanomater.* **2023**, *2023*, No. 5432099.
(105) Rajagopalan, K. K.; Sukhishvili, S. A. Temperature-and Creep-Resistant Diels−Alder Salogels for Shape Stabilization of Salt Hydrate Phase Change Materials. *J. Mater. Chem. A Mater.* **2025**, *13* (11), 8157−8170.
(106) Shahbaz, K.; AlNashef, I. M.; Lin, R. J. T.; Hashim, M. A.; Mjalli, F. S.; Farid, M. M. A Novel Calcium Chloride Hexahydrate-Based Deep Eutectic Solvent as a Phase Change Materials. *Sol. Energy Mater. Sol. Cells* **2016**, *155*, 147−154.
(107) Jafari, K.; Fatemi, M. H.; Estellé, P. Deep Eutectic Solvents (DESs): A Short Overview of the Thermophysical Properties and Current Use as Base Fluid for Heat Transfer Nanofluids. *J. Mol. Liq.* **2021**, *321*, No. 114752.
(108) Lu, Z.; Wang, S.; Ying, H.; Liu, B.; Jia, W.; Xie, J.; Sun, Y. Preparation and Thermal Properties of Eutectic Phase Change Materials (EPCMs) with Nanographite Addition for Cold Thermal Energy Storage. *Energy* **2024**, *290*, No. 130148.
(109) Atilhan, M.; Aparicio, S. Molecular Dynamics Simulations of Metal Nanoparticles in Deep Eutectic Solvents. *J. Phys. Chem. C* **2018**, *122* (31), 18029−18039.
(110) Dehury, P.; Singh, J.; Banerjee, T. Thermophysical and Forced Convection Studies on (Alumina + Menthol)-Based Deep Eutectic Solvents for Their Use as a Heat Transfer Fluid. *ACS Omega* **2018**, *3* (12), 18016−18027.
(111) Walvekar, R.; Chen, Y. Y.; Saputra, R.; Khalid, M.; Panchal, H.; Chandran, D.; Mubarak, N. M.; Sadasivuni, K. K. Deep Eutectic Solvents-Based CNT Nanofluid − A Potential Alternative to Conventional Heat Transfer Fluids. *J. Taiwan Inst. Chem. Eng.* **2021**, *128*, 314−326.
(112) Ayres, L. B.; Bandara, M.; McMillen, C. D.; Pennington, W. T.; Garcia, C. D. EutXG: A Machine-Learning Model to Understand and Predict the Melting Point of Novel X-Bonded Deep Eutectic Solvents. *ACS Sustainable Chem. Eng.* **2024**, *12* (30), 11260−11273.
(113) Abbas, U. L.; Zhang, Y.; Tapia, J.; Md, S.; Chen, J.; Shi, J.; Shao, Q. Machine-Learning-Assisted Design of Deep Eutectic Solvents Based on Uncovered Hydrogen Bond Patterns. *Engineering* **2024**, *39*, 74−83.
(114) Mohan, M.; Jetti, K. D.; Smith, M. D.; Demerdash, O. N.; Kidder, M. K.; Smith, J. C. Accurate Machine Learning for Predicting the Viscosities of Deep Eutectic Solvents. *J. Chem. Theory Comput.* **2024**, *20* (9), 3911−3926.
(115) Santos, J. P.; Sosa, F. H. B.; Abranches, D. O.; Coutinho, J. A. P. Artificial Intelligence in the Discovery of Deep Eutectic Solvents with Lubricant Applications. *ACS Omega* **2025**, *10* (37), 43024−43033.

https://doi.org/10.1021/acsaem.5c02743
ACS Appl. Energy Mater. XXXX, XXX, XXX−XXX